ELSEVIER

Journal of Chromatography A, 978 (2002) 81–107

JOURNAL OF CHROMATOGRAPHY A

www.elsevier.com/locate/chroma

Comparison of the adsorption equilibrium of a few low-molecular mass compounds on a monolithic and a packed column in reversed-phase liquid chromatography

F. Gritti[a,b], W. Piatkowski[a,b,1], G. Guiochon[a,b,*]

[a]*Department of Chemistry, The University of Tennessee, Knoxville, TN 37996-1600, USA*

[b]*Division of Chemical and Analytical Sciences, Oak Ridge National Laboratory, Oak Ridge, TN, USA*

Received 17 June 2002; received in revised form 12 August 2002; accepted 16 August 2002

Abstract

Adsorption isotherm data were acquired by frontal analysis for several low-molecular mass compounds (3-phenyl 1-propanol, 4-*tert*.-butylphenol, butylbenzene, and butyl benzoate) on a classical packed column and a monolithic column using methanol–water RP-HPLC conditions. These columns have similar characteristics (C_{18}-bonded silica, close specific surface areas and bonding densities). In each case, the isotherm model best accounting for the data was the same on both columns. The solute polarity determines the class of this model. For the two –OH compounds it was a Langmuirian adsorption isotherm. The hydrocarbon data were best modeled by an anti-Langmuir convex-downward isotherm model. The adsorption data for the aromatic ester exhibited a nearly linear behavior, depending on the methanol concentration of the mobile phase. A slightly convex downward isotherm was obtained at high methanol concentrations while the best fitting was obtained with a liquid–solid extended multilayer B.E.T. isotherm model at low concentrations. The validation of these models is discussed in detail. In all cases, similar values of the adsorption–desorption constants were found, underlining the closeness of the adsorption energies on both columns. By contrast, the adsorption capacity of the monolithic column was found to be approximately 1.4 greater than that of the packed column in spite of the close values of the surface areas of the silica in both columns.

Keywords: Adsorption isotherms; Monolithic columns; Frontal analysis; Isotherm modeling; Adsorption equilibrium; Extended liquid–solid B.E.T. model

1. Introduction

Considerable increases in column efficiency and/or reductions in analysis time were made in the 1970s by reducing the average size of the particles of the conventional spherical packing materials [1–3]. Because these gains were inevitably accompanied by severe increases in the column pressure drop, this trend has abated for the last 20 years and the most efficient columns that can be used in practice are limited to 25-cm long columns packed with particles of an average diameter of 3 μm. The recent advent

*Corresponding author. Tel.: +1-865-974-0733; Fax: +1-865-974-2667.

E-mail address: guiochon@utk.edu (G. Guiochon).

[1]On leave from the Faculty of Chemistry, Rzeszów University of Technology, W. Pola 2 Street, 35-959 Rzeszów, Poland.

0021-9673/02/$ – see front matter
PII: S0021-9673(02)01279-7

of commercially available monolithic columns, made of a single piece of solid adsorbent material [4–10], offers new practical possibilities for trading short retention times for very high efficiencies while escaping to a degree the pressure constraint. The lower hydraulic resistance of monolithic columns is related to their much higher external porosity that is itself reflected by their higher total porosity (0.80–0.99 instead of 0.50–0.7 for the packed columns). Another related advantage of monolithic columns is that they give low HETPs at high flow-rates, allowing reductions in analysis times [11–14].

In principle, monoliths could be made of synthetic organic materials (e.g., acrylate resins), of natural polymers (cellulose), or of inorganic materials such as silica. The only commercial available monolith [11,12], however, is based on the work carried out by Tanaka and co-workers [4–10] and belongs to this last type. Its manufacturing is based on a sol–gel process which includes the hydrolysis and polycondensation of alkoxysilanes (e.g., tetramethoxysilane or tetraethoxysilane) in the presence of water-soluble polymers (e.g., poly(ethyleneoxide) or polyethylene glycol) [4]. Tanaka and co-workers [5–7] showed that the amount of polymer dissolved in the alkoxysilane medium controls independently the size distributions of the through-macropores and of the mesopores of the silica skeleton. This is critical because the former are equivalent to the interstitial volume that controls bed permeability in packed columns while the latter is equivalent to the spherical particle whose size controls the mass transfer kinetics, hence the column efficiency. Furthermore, the average size of the mesopores in the skeleton, hence the surface area available for solute adsorption and their retention, can be adjusted by treating the gel with specific concentrations of aqueous ammonium hydroxide solution. The limiting step in the fabrication of silica monoliths stems from the slow rate at which the gel must be dried. Cylindrical monoliths dried too fast exhibit radial heterogeneity, resulting in a low column efficiency and a fragile silica rod. Consequently, the preparation of monoliths wider than a few millimeters is difficult and long. Only analytical columns are now commercially available. Everything else being constant, the time that it takes to dry a monolith is proportional to the square of its diameter. This leaves little hope for the early availability of preparative size monoliths.

The repeatability and reproducibility of retention data and band profiles, on a series of six Chromolith Performance RP-18e columns from Merck (Darmstadt, Germany), were carried out by Kele and Guiochon [15]. Made of a C_{18} chemically bonded silica and belonging to six different production batches, these columns exhibited a high degree of repeatability. This study confirmed the advantages of monolithic columns over conventional packed ones, they have a lower separation impedance, i.e., require a much lower head pressure to achieve a given column higher efficiency. Their availability makes possible high-speed chromatography. Fast separations of biological macromolecules such as proteins and polynucleotides [16] or of smaller biomolecules [17], the fast analysis of the metabolites of drugs [18,19], the rapid preparative isolation of cyclosporin [20], the fast separation of drug intermediate diastereoisomers [21] or of peptide toxins [22] have been successfully carried out.

The goal of this work is to compare the surface properties of monolithic and particle-packed columns, not from the perspective of analytical columns, operating at low concentrations, under linear conditions, but from a preparative viewpoint, by operating under nonlinear conditions. We compare isotherm data acquired on a classical packed column (Symetry C_{18} from Waters) and the only commercially available monolithic column (Chromolith Performance RP-18e from Merck). Cavazzini et al. [23] showed recently that the adsorption isotherms of butyl- and amyl-benzene on the Chromolith Performance column were clearly convex downward, a rather unusual isotherm behavior in liquid–solid equilibrium. Obviously, it was important to check whether this was a general property of C_{18}-bonded silica surfaces or whether it was specific of the monolithic column. More generally, we need to know if there are significant differences between the adsorption thermodynamics and kinetics of the columns belonging to these two different types. For this purpose, four solutes with widely different physicochemical properties were chosen, in order to generate distinct thermodynamic behaviors. Their isotherm data on both columns were acquired by frontal analysis and modeled. These models were validated

by comparing the experimental and calculated profiles of overloaded elution bands.

2. Theory

2.1. Determination of single-component isotherms

Among the various chromatographic methods available to determine single-component isotherms, frontal analysis (FA) is the most accurate [24,25]. It consists in quickly replacing the stream of mobile phase percolating through the column with solutions of the studied compound of increasing concentrations and recording the breakthrough curves at the column outlet. Mass conservation of the solute between the time when the new solution enters the column and a final time for which the plateau concentration is reached allows the calculation of the adsorbed amount, q^*, of solute in the stationary phase at equilibrium with a given concentration, C, in the mobile phase. Area A_2 in Fig. 1 represents this amount. This area is best measured by integration of the breakthrough curve (equal area method). The area on the left of the breakthrough curve ($A_1 + A_2$) is the mass of solute constantly present in the column, i.e., the sum of the mass of solute in the mobile phase occupying the column void-volume (A_1) and the mass of solute adsorbed in the stationary phase (A_2). The adsorbed amount q^* is given by:

$$q^* = \frac{C(V_{eq} - V_0)}{V_a} \quad (1)$$

where V_{eq} and V_0 are the elution volume of the equivalent area and the hold-up volume, respectively, and V_a is the volume of stationary phase.

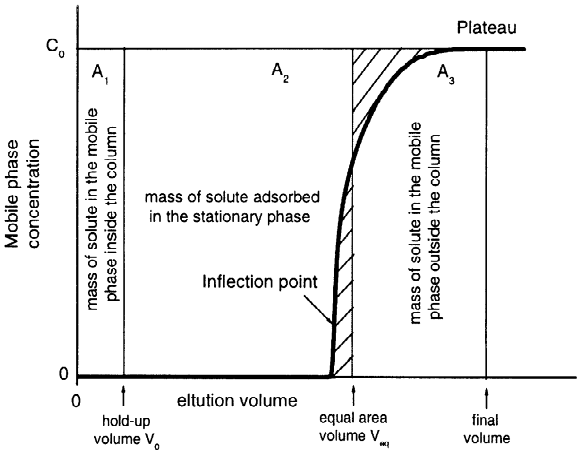

Fig. 1. Frontal analysis method of determination of the equilibrium concentrations in the stationary phase. The breakthrough curve is represented by the thick solid line. The two-hatched surfaces on the right and left side of the breakthrough curve have the same area and fix the volume of equivalent area used for the calculation. A large error may be made if the inflection point is considered.

2.2. Models of isotherms

The data points $(q^*,c)_i$ (i = number of FA concentration steps) were fitted to different models of adsorption isotherms for liquid–solid equilibrium. We describe here the models used in this work.

2.2.1. The Langmuir isotherm

This is the model most frequently used in the study of liquid–solid chromatographic processes, in spite of its empirical nature [24,25]. Writing that, at equilibrium, the rates of desorption (kinetic constant k_d) and adsorption (kinetic constant k_a) of the adsorbate molecules are equal and assuming a first order kinetic gives:

$$q^* = q_s \frac{bC}{1 + bC} \quad (2)$$

where q_s is the specific saturation capacity of the adsorbent or total number of adsorption sites per unit volume of the adsorbent and $b = k_a/k_d$ is the adsorption–desorption equilibrium constant on the solid surface. At low concentrations, the Henry constant H is equal to $q_s b$.

2.2.2. The parabolic isotherm

At low concentrations, any isotherm can be replaced by its two-term expansion. This is referred to as the parabolic isotherm [24,26]. This model can be used as an empirical model to describe slightly convex upward or downward isotherms. It is useful when a low saturation concentration of the mobile phase prevents from measuring isotherm data in a wide enough concentration range accurately to model the isotherm. The expansion of the Langmuir model is:

$$q^* = HC(1 - bC) \quad (3)$$

where H is the Henry constant and $0 < b \ll 1$ for a slightly convex upward isotherm.

2.2.3. The anti-Langmuir isotherm

This empirical model is often used to describe convex downward isotherms in gas– or liquid–solid equilibrium [23]. This model assumes that there is an infinite amount of adsorbate in the stationary phase when the concentration in the mobile phase is $1/b$, which is an unrealistic situation. In practice, this concentration cannot be approached in liquid–solid equilibria, a case in which there is no phenomenon equivalent to capillary condensation observed in gas–solid equilibria. The model constant $1/b$ must thus be considered as an empirical parameter. The equation of this model is:

$$q^* = \frac{HC}{1 - bC} \quad (4)$$

where $b > 0$ and H is the Henry constant.

2.2.4. The Langmuir anti-Langmuir isotherm (LaL)

The empirical biLangmuir and Langmuir/anti-Langmuir (LaL) isotherms were also suggested for a heterogeneous surface with two different kinds of sites that behave independently.

In the LaL model which is the only of the two used in this work, adsorption on one part of the surface is described by a classical Langmuir isotherm while adsorption on the complementary part of the surface follows anti-Langmuir isotherm behavior. This model can be expressed as follows:

$$q^* = q_{s,1} \frac{b_1 C}{1 + b_1 C} + \frac{H_2 C}{1 - b_2 C} \quad (5)$$

an equation that can be recast as the ratio of two second-order polynomials:

$$q^* = \frac{(b_1 q_{s,1} + H_2)C + (b_1 H_2 - b_2 H_1)C^2}{1 + (b_1 - b_2)C - b_1 b_2 C^2} \quad (6)$$

This equation is clearly different from that of the second-order statistical thermodynamic model of adsorption (or quadratic isotherm [24]) that accounts for adsorption isotherm data exhibiting a horizontal asymptote corresponding to a saturation capacity at an infinite concentration and a possible inflection point at intermediate concentrations.

At low concentration, this isotherm is linear and the overall Henry constant is simply the sum of the Henry constant of the two contributions, $H_1 = q_s b_1$ and H_2. The constant b_1 is consistent with the adsorption–desorption equilibrium constant of the adsorbate solute on the first part of the surface (Langmuirian). As for the anti-Langmuir isotherm, this isotherm model is valid only for concentrations below $1/b_2$.

2.2.4. The virial isotherm

The virial isotherm is widely used in gas–solid adsorption equilibrium [27,28], especially to derive accurate values of the Henry constant from experimental data by extrapolation of these data to the low partial pressure range which may not be available for measurements. It is derived in gas–solid adsorption from the Gibbs adsorption isotherm from thermodynamics [25]:

$$\frac{bP}{n_{ads}} = \exp\left(2A_1 n_{ads} + \frac{3}{2} A_2 n_{ads}^2 + \cdots\right) \quad (7)$$

where A_1 and A_2 are the first two coefficients of the virial development, n_{ads} is the number of moles of solute adsorbed on the solid surface, and P the solute pressure in the gas phase.

As was done for many other gas–solid isotherm models, we propose to extend this isotherm model to liquid–solid equilibrium, assuming that the intrinsic competitive adsorption of the molecules of the mobile phase components is negligible, i.e., that the adsorbate molecules are more strongly adsorbed than those of the solvents. Identifying the pressure P to the adsorbate concentration, C, and b to the Henry constant, H, when n_{ads} tends towards zero, $n_{ads}/V_a = q^*$, and:

$$\frac{HC}{q^*} = \exp(A_1' q^* + A_2' q^{*2}) \quad (8)$$

where A_1' and A_2' are the new parameters for the characterization of the non-linear behavior of the isotherm in the liquid–solid system.

2.2.4. The Fowler-Guggenheim/Jovanovic-Freundlich (FG/JF) isotherm

This model accounts for the adsorption of a compound on a heterogeneous surface and for adsor-

bate–adsorbate interactions. The single-component FG/JF isotherm model is given by the following equation [29]:

$$\frac{q^*}{q_s} = 1 - \exp\left(-\left(bC \exp\left(\alpha \frac{q^*}{q_s} \right)^{\upsilon} \right) \right) \quad (9)$$

where q_s is the saturation capacity, b is analogous to an equilibrium constant between the solute and the stationary phase (at infinite dilution, the Henry constant is given by $q_s b$), α relates to the energy of lateral interaction between solute molecules and ν is the heterogeneity parameter (with $0 < n < 1$).

2.2.5. The liquid–solid extended B.E.T. isotherm

The Brunauer, Emmett, and Teller (B.E.T.) model is the most widely applied isotherm in gas–solid equilibrium. It accounts for multilayers adsorption [30]. It was developed to describe adsorption phenomena in which a second and then subsequent molecular layers of adsorbate form at pressures that are well below the pressure required for the completion of the monolayer. This model is used to extract the monolayer capacity and hence the surface area of many adsorbent surfaces [31]. The assumption made in this model is that each molecule in the first adsorbed layer provides an adsorption site for the second layer, and so on. Molecules in the second and subsequent layers are assumed to behave essentially as those in the bulk liquid. Assuming further a kinetic argument for the first layer adsorbed on the surface, the following B.E.T. equation is obtained:

$$q^* = \frac{q_s b P/P_s}{(1 - P/P_s)(1 - P/P_s + bP/P_s)} \quad (10)$$

where p_s is the vapor pressure of the liquid adsorbate at the relevant temperature, b the adsorption–desorption equilibrium constant on the solid surface and q_s the close-packed monolayer capacity.

In liquid–solid adsorption, we may assume that the mobile phase components are only weakly adsorbed on the solid surface while the solute is strongly adsorbed, the mobile phase components being considered as practically inert. Bartell and Donahue showed the existence of liquid systems displaying the B.E.T. isotherm [32]. This is the case, in NP-HPLC, of the adsorption of water from a benzene solution onto silica gel [33,34]. This situation may also arise in RP-HPLC when using a C_{18} stationary phase and a methanol–water solution as the mobile phase since the retention factor of methanol is about 1 in pure water [35] and necessarily less for mobile phases richer in methanol.

So, we assume a single component model with simultaneous solute adsorption equilibria for the first (adsorbate–adsorbent interactions represented by the equilibrium constant $b_S = k_S^a / k_S^d$) and for the subsequent layers (adsorbate–adsorbate interactions represented by the equilibrium constant $b_L = k_L^a / k_L^d$) as well as a finite number, N, of layers (Fig. 2). The variables are the surface coverage fractions, θ_0, θ_1, $\theta_2, \ldots \theta_i, \ldots \theta_n$. Of course, the summation of the surface coverage fractions is unity:

$$\theta_0 + \theta_1 + \theta_2 + \cdots + \theta_i + \cdots + \theta_n = \sum_{i=1}^{i=n} \theta_i = 1 \quad (11)$$

At equilibrium, a pseudo-steady-state is assumed and the equilibration kinetics written for each surface fraction becomes:

(1) For the free surface fraction, θ_0

$$\frac{\partial \theta_0}{\partial t} = 0 = k_S^d \theta_1 - k_S^a C \times (1 - \theta_1 - \theta_2 - \cdots - \theta_i - \cdots - \theta_n)$$

$$\text{or} \quad \theta_1 = b_S C (1 - \theta_1 - \theta_2 - \cdots - \theta_i - \cdots - \theta_n) \quad (12a)$$

(2) For the first layer, of surface coverage q_1, the same kinetic constraint is expressed as the sum of four terms:

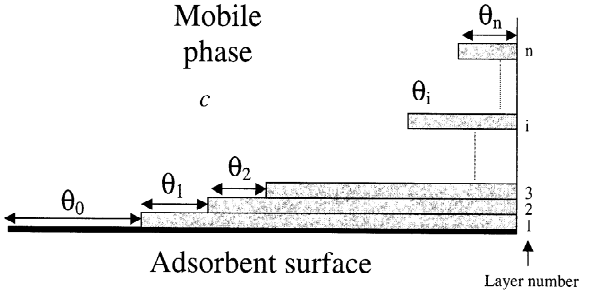

Fig. 2. Scheme of multilayer adsorption.

$$\frac{\partial\theta_1}{\partial t} = 0 = k_S^a C(1-\theta_1-\theta_2-\cdots - \theta_i-\cdots-\theta_n) - k_S^d\theta_1 - k_L^a C\theta_1 + k_L^d\theta_2$$
$$= -\frac{\partial\theta_0}{\partial t} - k_L^a C\theta_1 + k_L^d\theta_2 \quad \text{or} \quad \theta_2 = b_L C\theta_1 \tag{12b}$$

Similarly, we can successively derive the following equations:

$$\begin{aligned}&\theta_3 = b_L C\theta_2\\ &\cdots\\ &\theta_i = b_L C\theta_{i-1}\\ &\cdots\\ &\theta_n = b_L C\theta_{n-1}\end{aligned} \tag{12c}$$

Combining Eqs. (12a)–(12c) gives the total amount of the adsorbate in equilibrium with the mobile phase at concentration C (see Fig. 2):

$$q^* = q_s(\theta_1 + 2\theta_2 + 3\theta_3 + \cdots + i\theta_i + \cdots + n\theta_n)$$
$$= q_s\sum_{i=1}^{i=n} i\theta_i = q_s\theta_1\sum_{i=1}^{i=n} ix^{i-1} = q_s\theta_1\sum_{i=1}^{i=n}\frac{d}{dx}(x^i)$$
$$= q_s\theta_1\frac{d}{dx}\left(x\frac{1-x^n}{1-x}\right)$$
$$= q_s\theta_1\frac{1-(n+1)x^n+nx^{n+1}}{(1-x)^2} \tag{13}$$

with $x = b_L\ C < 1$. θ_1 is obtained through Eq. (12a) with $y = b_S\ C$.

$$\theta_1 = \frac{1}{y^{-1} + \dfrac{1-x^n}{1-x}} \tag{14}$$

Finally, the isotherm equation for a finite number of layers (n) is:

$$q^* = q_s\frac{1-(n+1)x^n+nx^{n+1}}{(1-x)^2\left(y^{-1}+\dfrac{1-x^n}{1-x}\right)} \tag{15}$$

If there is an infinite number of layers, this equation can be simplified and we obtain

$$q^* = q_s\frac{1}{(1-x)^2\left(y^{-1}+\dfrac{1}{1-x}\right)}$$
$$= q_s\frac{y}{(1-x)(1-x+y)}$$
$$= q_s\frac{b_S C}{(1-b_L C)(1-b_L C+b_S C)} \tag{16}$$

This equation has exactly the same mathematical form than the BET isotherm equation (Eq. (10)) derived in gas–solid adsorption. q_s and b_S have the same physical meaning. However, the parameter b_L in Eq. (16) does not have the same physical interpretation as $1/p_S$ in Eq. (10). By contrast, b_L is of the same nature as b_S, it is an equilibrium constant for surface adsorption–desorption (over a layer of adsorbate molecules) while p_S is a real asymptotic limit pressure, corresponding to the condensation of the adsorbate at the relevant temperature. Nevertheless, both parameters are related to the strength of the solute–solute interactions in a condensed state and this makes Eqs. (10) and (17) quite similar from a general physicochemical viewpoint.

2.3. Modeling of high-performance liquid chromatography

The profiles of overloaded elution bands were calculated using two models of non-linear chromatography, the equilibrium-dispersive model (ED) and the lumped pore diffusion model (POR) [24,25,36].

2.3.1. Equilibrium-dispersive model (ED model)

This model assumes instantaneous equilibrium between the mobile and the stationary phase but a finite column efficiency. The latter is assumed to originate from an apparent axial dispersion coefficient, D_a, accounting for all the dispersive phenomena (molecular, eddy, flow diffusions and non equilibrium effects as well) that take place in the column.

$$D_a = \frac{uL}{2N} \tag{17}$$

where u is the linear mobile phase velocity, L the column length, and N the number of theoretical plates or apparent efficiency of the column.

In this model, the mass balance equation for a single component is expressed as follows:

$$\frac{\partial C}{\partial t} + u\frac{\partial C}{\partial z} + F\frac{\partial q^*}{\partial t} - D_a\frac{\partial^2 C}{\partial z^2} = 0 \quad (18)$$

where q^* and C are the stationary and mobile phase concentrations of the adsorbate, respectively, t the time, z the distance along the column and $F = (1 - \varepsilon_T)/\varepsilon_T$ is the phase ratio, with ε_T the total column porosity. q^* is related to C through the isotherm equation, $q^* = f(C)$.

2.3.2. Lumped pore diffusion model (POR)

This model is more sophisticated than the ED model because it accounts in more detail for the mass transfer kinetics. Two mass balances are written for the single-component in the mobile phase, one in the stream percolating around the solid-phase particles, the second inside these particles (where the mobile phase is considered as stagnant):

$$\epsilon_e\frac{\partial C}{\partial t} + u\frac{\partial C}{\partial z} = \epsilon_e D_L\frac{\partial^2 C}{\partial z^2} - (1 - \epsilon_e)k_{ov}a_p(C - \bar{C}_p) \quad (19)$$

and

$$\epsilon_p\frac{\partial \bar{C}_p}{\partial t} + (1 - \epsilon_p)\frac{\partial \bar{q}}{\partial t} = k_{ov}a_p(C - \bar{C}_p) \quad (20)$$

where C is the solute concentration in the external mobile phase, $\bar{C}_p$ is the average solute concentration in the stagnant mobile phase inside the solid-phase, $\bar{q}$ is the average solute concentration adsorbed in the solid particle, ε_e is the external porosity, ε_p is the internal porosity related to ε_T by $\varepsilon_T = \varepsilon_e + (1 - \varepsilon_e)\varepsilon_p$, k_{ov} is the overall mass transfer coefficient between the mobile and the stationary phases and a_p the external surface area of the adsorbent particles relative to the particle volume ($a_p = 6/d_p$ for spherical particles). $\bar{q}$ is related to $\bar{C}_p$ through the isotherm equation $\bar{q} = f(\bar{C}_p)$. Considering the solute mass transfer in series from the external mobile phase to the mobile phase inside the particles (k_{ext}) and then to the solid surface (k_{int}), k_{ov} can be expressed as:

$$\frac{1}{k_{ov}} = \frac{1}{k_{ext}} + \frac{1}{k_{int}} \quad (21)$$

D_L in Eq. (19) is the axial dispersion coefficient in the mobile phase. It is calculated through Gunn equation [37], assuming that the variance distribution of the ratio between the fluid linear velocity and the average velocity over the column cross-section is zero. The Gunn equation is then:

$$\epsilon_e\frac{D_L}{d_p u} = \frac{\mathrm{Re\,Sc}}{4\alpha_1^2(1 - \epsilon_e)}(1 - p)^2 + \left(\frac{\mathrm{Re\,Sc}}{4\alpha_1^2(1 - \epsilon_e)}\right)^2 p(1 - p)^3 \times\left(\exp\left(\frac{-4\alpha_1^2 11(1 - \epsilon_e)}{p(1 - p)\mathrm{Re\,Sc}}\right) - 1\right) + \frac{\epsilon_e}{\tau\,\mathrm{Re\,Sc}} \quad (22)$$

where Re and Sc are the Reynolds and Schmidt numbers, defined by:

$$\mathrm{Re} = \frac{u d_p \rho}{\eta}$$

where d_p, ρ and η are the particle diameter in the packed column and the equivalent diameter of the through-pores in the monolithic column, the density and the viscosity of the mobile phase, respectively.

$$\mathrm{Sc} = \frac{\eta}{\rho D_m}$$

where D_m is the molecular diffusivity of the adsorbate in the mobile phase approximated by the Wilke–Chang equation [38] and extended to mixed solvents by Perkins and Geankoplis [39]:

$$D_m = 7.4 \times 10^{-8}\frac{T\sqrt{\phi M}}{\eta V_m^{0.6}} \quad (23)$$

where T is the absolute temperature, V_m the molal volume of the adsorbate at its normal boiling temperature. ϕM is calculated from the molar fractions x_A, x_B, the association factors ϕ_A, ϕ_B and the molecular mass M_A, M_B of the single components A and B of the mixed solvent

$$\phi M = x_A\phi_A M_A + x_B\phi_B M_B \quad (24)$$

Finally, in Eq. (22), α_1 is the first root of the zero Bessel function (2.4048), τ is the bed tortuosity factor equal to 1.4 according to Ref. [37], and p is a parameter defined by Ref. [37]:

$$P = -0.17 + 0.33\exp(-24/\mathrm{Re}) \quad (25)$$

This estimate of D_L is obviously an empirical one and, therefore, it is bound to be inaccurate at best, as already suggested by several authors [40–44].

2.3.3. Initial and boundary conditions for ED and POR models

For both model the same initial and boundary conditions were used. At $t=0$ the concentration of the adsorbate in the column is uniformly equal to zero inside the column and the stationary phase is in equilibrium with the pure mobile phase. The boundary conditions used are the classical Dankwerts-type boundary conditions [45] at the inlet and outlet of the column.

2.3.4. Numerical solutions of the POR model and ED model

The ED and POR models were solved using a computer program based on an implementation of the method of orthogonal collocation on finite elements [46–48]. The set of discretized ordinary differential equations was solved with the Adams–Moulton method, implemented in the VODE procedure [49]. The relative and absolute errors of the numerical calculations were 1×10^{-6} and 1×10^{-8}, respectively.

3. Experimental

3.1. Chemicals

The different mobile phases used in this work, whether for the determination of the adsorption isotherms data or for the elution of large size bands were mixtures of HPLC-grade water and methanol, both purchased from Fisher Scientific (Fair Lawn, NJ, USA). Acetonitrile, used to wash the columns between each frontal analysis measurement, was bought from the same supplier. The solvents used to prepare the mobile phase were filtered before use on SFCA filter membrane 0.2 μm pore size (Suwannee, GA, USA). All the solutes uracil, 3-phenyl-1-propanol, 4-*tert*.-phenol, butyl benzoate and amylbenzene were all obtained from Aldrich (Milwaukee, WI, USA).

3.2. Materials

The monolith column is a Chromolith Performance RP-18e, 100×4.6 mm, column, C_{18} bonded and endcapped (Ref. #23, Merck). It is one of the lot of six columns used by Kele and Guiochon [15] for their study on the repeatability of the chromatographic properties of these columns, by Al-Bokari et al. [50] for the determination of the internal and external porosities of monolithic columns, and by Cavazzini et al. [23] to investigate the adsorption data of butylbenzene.

The packed column is a Symetry C_{18} column, 150×3.9 mm, endcapped (Ref. #5 Milford, MA, USA). It is one of the lot of 15 columns used by Kele and Guiochon [51] for their study of the repeatability of the chromatographic properties of these columns.

The hold-up times of these two columns were determined from the retention time of uracil injections. The mean of at least four consecutive readings, agreeing to within 1% was taken for each mobile phase used (see Fig. 3).

The physico-chemical properties of each column, as supplied by the manufacturer (Merck and Waters) are listed in Table 1. The external porosities were obtained from Ref. [50] for the monolith column ($\epsilon_e=0.706$) and the packed column ($\epsilon_e=0.37$).

3.3. Apparatus

The data were acquired using a Hewlett-Packard (Palo Alto, CA, USA) HP 1090 liquid chromatograph. This instrument includes a multi-solvent delivery system (tank volume, 1 dm^3 each), an auto sampler injection with a 25-μl loop, a diode-array UV-detector, a column thermostat and a computer data acquisition station. Compressed nitrogen and helium bottles (National Welders, Charlotte, NC, USA) are connected to the chromatograph instrument to allow the continuous operation of the pump and auto sampler systems.

3.4. Isotherm measurements

The measurements were carried out at a constant temperature of 23 °C. Just prior any isotherm determination, a calibration curve is recorded for the

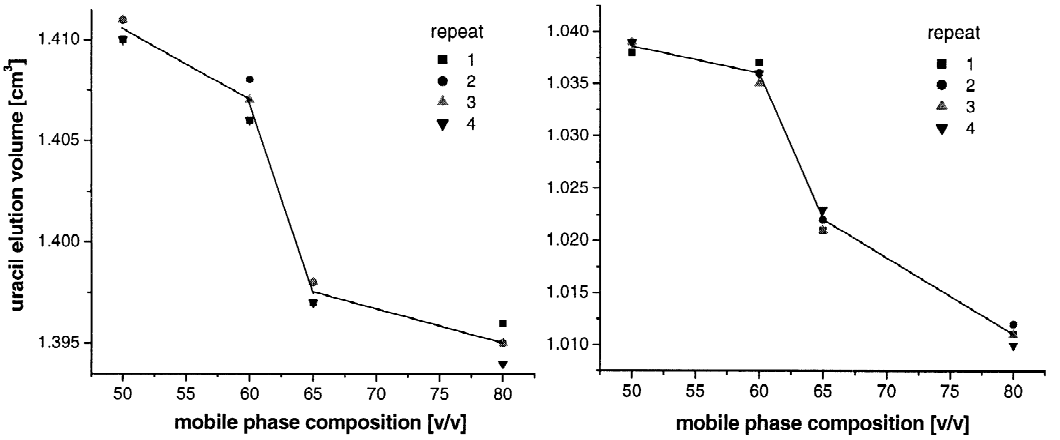

Fig. 3. Plot of the elution volume of uracil on the monolithic (left) and the packed (right) columns versus the mobile phase composition (methanol–water).

solute at the chosen wavelength. Thirty-five concentration points are acquired, uniformly distributed within the concentration range investigated. The nonlinear calibration data are fitted to a third-degree polynomial.

All isotherm data were obtained by frontal analysis. One pump of the HPLC instrument delivered a stream of the pure mobile phase, the second pump the pure sample solution. The desired concentration of the studied compound is obtained by selecting the concentration of the mother sample solution and the flow-rate fractions delivered by the two pumps. The breakthrough curves are recorded successively at a flow-rate of 1 ml/min, with a sufficiently long time delay between each breakthrough curve to allow sufficient time for the reequilibration of the column with the pure mobile phase. The injection time of the sample depends on the time required to reach the plateau concentration at the outlet of the column.

All the overloaded profiles needed for the validation of the fitted isotherms were recorded during the frontal analysis experiments.

Table 1
Physico-chemical properties of the packed (Waters) and monolithic (Merck) silica columns supplied by the manufacturers

	Packed	Monolith
Particle size	5 μm	–
Skeleton size	–	1.3–1.6 μm
Interparticle pore size	1.25–2 μm	–
Macropore size	–	2 μm
Mesopore size	90 Å	130 Å
Surface area	340 m^2/g	300 m^2/g
Surface coverage (C_{18})	3.2 $\mu mol/m^2$	3.6 $\mu mol/m^2$
Total porosity	0.65	>0.80
Total carbon	18%	19.5%
Endcapping	Yes	Yes

4. Results and discussion

4.1. Hold-up and adsorbent volumes determination

In order to measure the concentration q^* of the adsorbate in the stationary phase (i.e., the amount of the compound adsorbed per unit volume of stationary phase), we need the volume occupied by the stationary phase, V_a in presence of the mobile phase. Note that q^* is not an actual concentration because the molecules of adsorbate are located on the surface of the silica material. The main difficulty of this determination is to decide where is the boundary between the stationary and the mobile phase. We assumed in this work that V_a is the volume complementary of the elution volume, V_0, of a non-retained compound that can access to the whole surface area of the solid silica material (i.e., $V_a = V_G - V_0$, where V_G is the geometrical volume of the column tubing).

Fig. 3 shows plots of the hold-up volumes, V_0, after correction for the extra-column volumes versus

the mobile phase composition. Uracil is considered as a non-retained compound in reversed-phase HPLC with methanol–water solutions as the mobile phase and is often used to determine hold-up volumes in RP-HPLC [52]. For both the monolithic and the packed column, the elution volume of uracil decreases with increasing concentration of methanol in the mobile phase (Fig. 3). This is explained by the swelling of the bonded C_{18} chains due to their increasing solubility in a solvent of increasing concentration in the organic solvent (MeOH). Accordingly, the volume available to the mobile phase decreases. The average values, $\overline{\epsilon_T}$, of the total porosities of the two columns are 0.844 for the monolithic and 0.570 for the packed column in the concentration range investigated. The first value is in good agreement with the results of two previous determinations, the one supplied by the manufacturer ε_T larger than 0.8) and the external porosity determined separately by inverse size-exclusion chromatography [50] in THF ($\varepsilon_T = 0.850$) for the same column [23]. The value for the packed column is consistent with the porosity $\varepsilon = 0.65$ reported by the manufacturer for the initial silica (i.e., before bonding of the C_{18} chains), based on multipoint nitrogen sorption. Our result of $\varepsilon_T = 0.570$ is consistent, given the relatively large carbon content of the bonded phase. It was confirmed by the results of similar measurements made latter on two identical Symmetry columns (columns #2 and #6 in [51]) for which $\varepsilon_T = 0.570$.

The relative decrease of the hold-up volume when the composition of the mobile phase changes from 50:50 to 80:20 (v/v) methanol–water is 1.1% for the monolith and 2.7% for the packed column. It is smaller for the monolithic column mainly because it has a higher hold-up volume (1.401 versus 1.024 cm^3). We note, however, that the increase of the volume occupied by the C_{18} chains (when [MeOH] increases from 50 to 80%) can be calculated from the data in Fig. 3a,b. It is approximately 15 and 27 μl for the monolithic and the packed column, respectively. But the number of C_{18} chains per gram of solid stationary phase is equivalent for the two columns (1080 and 1090 μmol/g, data supplied by the two manufacturers) while the volume of stationary phase contained in the column is nearly three times lower in the monolithic than in the packed column (0.259 and 0.766 cm^3). If we assume the same density for both silica materials, we must conclude that there are three times fewer alkyl chains in the monolithic column, which means that these chains expand on the average 50% more in the monolithic column than in the packed one, a result that we cannot explain without assuming that the mobile phase does not have access to the whole surface area in the packed column.

4.2. Isotherm of 3-phenyl-1-propanol

Because of the high solubility of 3-phenyl-1-propanol in methanol, its isotherm was measured in a water-rich mobile phase (50:50, v/v), in order to achieve a sufficiently long retention time on both columns, hence a good accuracy of the measurements of equilibrium data. The maximum solute concentration used was 20 g/dm^3. The retention factors at infinite dilution, k_0', was 5.38 and 1.92 on the packed and monolith column, respectively. The retention factor is related to the phase ratio, F, and the Henry constant, H:

$$k_0' = \frac{1 - \epsilon_T}{\epsilon_T} H = FH \tag{26}$$

To compare the retention on the two columns and eliminate the spurious influence of the large differences between their total porosities, we have to calculate the Henry constant. The phase ratios of the two columns being 0.748 (packed column) and 0.185 (monolithic column), we find that the Henry constant is significantly higher with the monolithic column (10.4 versus 7.2).

The two isotherms are clearly convex upward on the full range of solute concentration, as shown in Fig. 4. They fit well to a Langmuir isotherm. This result is consistent with the classical front shock (constant pattern for adsorption) and diffuse rear boundary (controlled by the kinetics of equilibration) on the breakthrough curves. The best fitting parameters are reported in Table 2. We found similar values for the binding constant (parameter b), i.e., 0.0382 and 0.0397 dm^3/g for the monolithic and the packed column, respectively. This close agreement suggests that the adsorption energy of 3-phenyl-1-propanol is equivalent on both columns, which confirms the fact

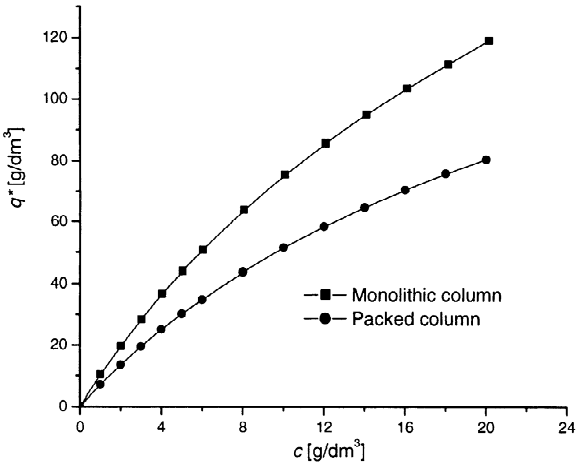

Fig. 4. Experimental isotherm of 3-phenyl-1-propanol on the monolithic and the packed columns with methanol–water (50:50, v/v) as the mobile phase. $T = 295$ K.

that identical surface chemistry was involved on these materials. Obviously, since the saturation capacity, q_S, and the binding constant, b_S, are related to the Henry constant ($H = q_S b_S$), a higher saturation capacity is found for the monolithic column, 272 g/dm^3 versus 181 g/dm^3 for the packed silica particles.

These values are consistent with other characteristics of the two columns. A saturation capacity of 272 g/dm^3 for 3-phenyl-1-propanol (MW = 136.20) on the monolithic column corresponds to 2 mol/dm^3. Assuming a density of 2.2 for silica, this gives a saturation capacity of $2\times10^3/2.2 = 910$ μol/g or 3.0 μmol/m^2 while the density of the bonded C_{18} chains is 3.6 μmol/m^2, meaning that eight molecules of the alcohol are adsorbed for 10 C_{18} chains. The same calculation gives for the packed column a saturation capacity of 1.7 μmol/m^2 and a chain density of 3.2 μmol/m^2, or five molecules of the alcohol adsorbed for 10 bonded C_{18} chains. These values appear to be reasonable although the significant difference between the behavior of the two columns appears surprising. It might hide a phenomenon specific to one or the other stationary phase.

4.3. Isotherms of 4-tert.-butyl-phenol

The isotherms of 4-*tert*.-butyl-phenol were measured at a higher methanol concentration (60:40, v/v) because its retention was too large with a 50:50 solution. The maximum solute concentration used was 16 g/dm^3. The retention factors at infinite dilution, k_0', are 6.52 and 2.61 on the packed and the monolithic column, respectively. These values are close to those observed for 3-phenyl-1-propanol in the poorer 50:50 solution. As for the alcohol, the Henry constant at infinite dilution is found higher on the monolithic column (Monolith = 14.1) than on the packed one (Packed = 8.7).

The shape of the equilibrium isotherms is convex upward on both columns and the data fit well again to a Langmuir model (Fig. 5). As in the previous case, nearly the same numerical value is obtained for the equilibrium constant, b, on the two columns, 0.0648 and 0.0619 dm^3/g for the monolithic and the

Table 2
Best isotherm parameters and standard deviations (%) obtained by regression analysis on packed and monolithic column for a Langmuir, parabolic and anti-Langmuir models[a]

Model	Compound	MP (v/v)	Packed	r^2	Monolithic	r^2
Langmuir	3-Phenyl-1-propanol	50:50	$q_S = 181\pm1\%$ $b_S = 0.0397\pm1\%$	0.9999	$q_S = 272\pm1\%$ $b_S = 0.0382\pm1\%$	0.9999
	4-*tert*.-Butylphenol	60:40	$q_S = 141\pm1\%$ $b_S = 0.0619\pm1\%$	0.9999	$q_S = 218\pm1\%$ $b_S = 0.0648\pm2\%$	0.9999
Parabolic	Butyl-benzoate	80:20	$H = 3.50\pm0.2\%$ $b_P = 0.0034\pm10\%$	0.9999	$H = 4.93\pm0.5\%$ $b_P = 0.022\pm6\%$	0.9999
Anti-Langmuir	Butyl-benzene	80:20	$H = 6.66\pm2.5\%$ $b_{aL} = 0.017\pm7\%$	0.9988	$H = 9.50\pm1\%$ $b_{aL} = 0.022\pm3\%$	0.9982

[a] The regression coefficient squared (r^2) is given. MP, mobile phase.

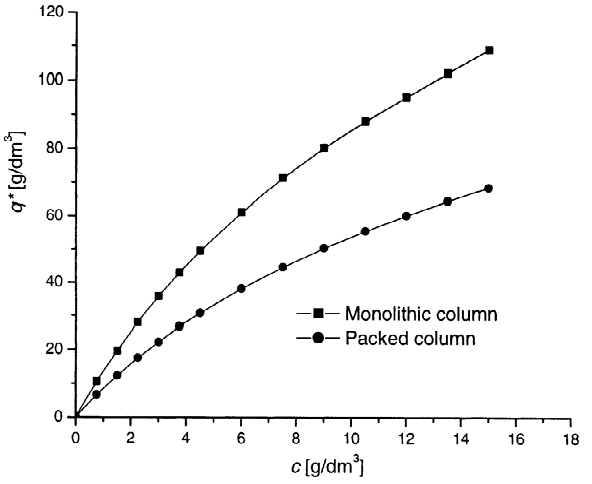

Fig. 5. Experimental isotherm of 4-*tert.*-butylphenol on the monolithic and the packed columns with methanol–water (60:40, v/v) as the mobile phase. $T = 295$ K.

packed columns, respectively. The relative difference is less than 5%. Despite a mobile phase richer in methanol, b is larger for 4-*tert.*-butylphenol than for 3-phenyl-1-propanol. This can be explained by the stronger hydrophobic interactions between the C_{18} chains and the more voluminous *tert.*-butylphenyl group than with the phenylpropyl group. The saturation capacities are again significantly different for the two columns. The best values derived are 218 g/dm^3 for the monolith and 141 g/dm^3 for the packing particles. The numbers of molecules of 4-*tert.*-butylphenol adsorbed at saturation are approximately six and four for 10 bonded C_{18} chains, respectively.

These results suggest that the position of the hydroxyl group on the hydrocarbon skeleton does not have a critical influence on the shape of the equilibrium isotherm. The solute probably positions at the interface with its hydrophobic part interacting with the C_{18} chains and its polar group solvated by the methanol–water solvent, which hinders subsequent solute–solute interactions in the adsorbed phase.

4.4. Isotherm of butylbenzene

In an earlier study, Cavazzini et al. [23] found that the equilibrium convex of butyl- and amyl-benzene on the Chromolith Performance column were concave upward and fitted well to an anti-Langmuir model. The only reasonable explanation for such a behavior is to be found in solute–solute interactions in the adsorbed phase. We repeated the earlier FA measurements [23] on the same packed column with the same methanol–water mobile phase (80:20, v/v) and obtained similar results. The maximum concentration used was 17 g/dm^3, it is close to the maximum solubility of the hydrocarbon in the mobile phase. The retention factor at infinite dilution, k_0', was then 5.72 and 2.17 on the packed and monolith column, respectively. The shape of the adsorption isotherm is concave upward on both the monolithic and the packed column, as demonstrated by the plot of q^*/C as a function of C which increases constantly within the range of concentrations accessible to measurements. This is also confirmed by the diffuse boundary at the front and the shock layer at the rear of the breakthrough curves.

The experimental data do not fit to the anti-Langmuir isotherm model as well as the data of the previous compounds fit to the Langmuir model. more specifically, there is a significant difference between the values of the Henry constant obtained from analytical data (retention time at infinite dilution) and from the best coefficient derived from the fit of the whole set of isotherm data. There values are Packed = 7.64 and 6.66 and Monolith = 10.5 and 9.5 for the analytical and the isotherm results, respectively. In both cases, the use of the anti-Langmuir model leads to an underestimation of the true value of the Henry constant (see Table 2). As shown in Fig. 6, the amount adsorbed at equilibrium with a given mobile phase concentration is again larger on the monolithic column than on the packed column. The same ratio of 1.4 is found between the two sets of data as it was for the alcohol and the phenol.

This result suggests that the polarity of the solute influences largely the shape of the equilibrium isotherm. The alcohol and the phenol interact rather strongly with both the mobile and the stationary phase and experience little solute–solute interactions in the adsorbed phase. By contrast, a hydrocarbon interacts little with the mobile phase but undergoes rather strong solute–solute interactions, leading to an anti-Langmuir or at least a convex downward isotherm. Finally, it is important to underline that, in all cases, independently of the polarity of the solute, the

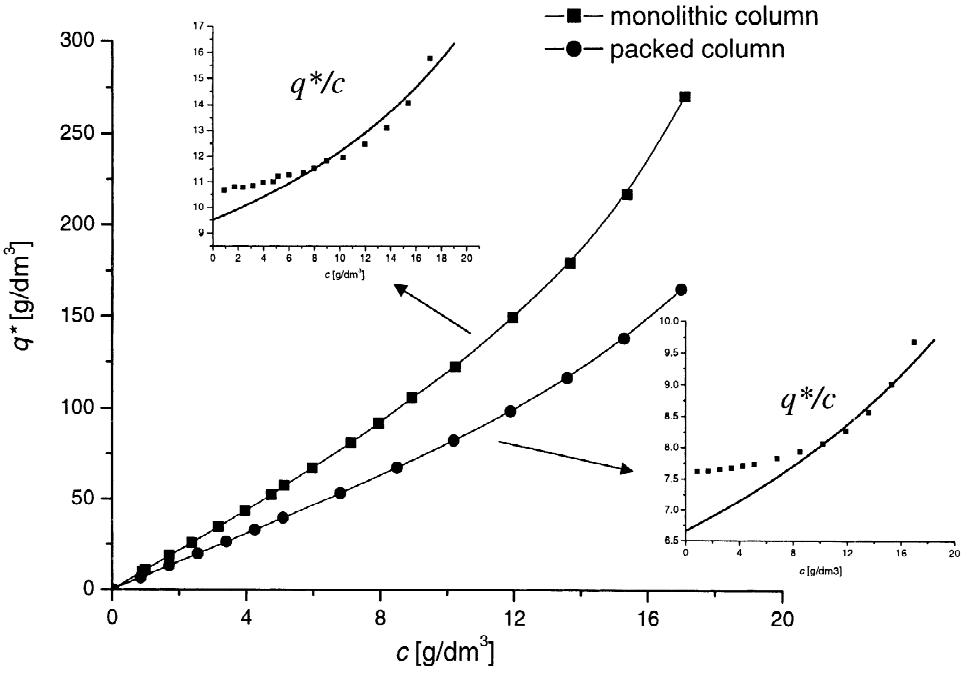

Fig. 6. Experimental isotherm of butylbenzene on the monolithic (data from Cavazzini et al. [23]) and the packed columns with methanol–water (80:20, v/v) as the mobile phase. Inserts: plots of q^*/C versus C for both columns, confirming their anti-Langmuir behavior. $T = 295$ K.

amount adsorbed at a given solute concentration in the mobile phase is approximately 40% larger on the monolithic column than on the packed column.

4.5. Isotherms of butylbenzoate

The polarity of butylbenzoate is intermediate between those of the two hydroxyl compounds and that of the hydrocarbon discussed earlier and so is the energy of the hydrogen-bond interactions that it gives with the methanol–water mobile phase. Butylbenzoate is only a good hydrogen-bond acceptor, attracting hydrogen atoms from the solvent with the two *n*-electron pairs available on its two oxygen atoms, in contrast with –OH derivatives that are not only good hydrogen-bond acceptors but also good hydrogen-bond donors because of mobility of the hydrogen atom of the hydroxyl function. Butylbenzene is not a hydrogen bond-donor and is a poor hydrogen-bond acceptor. It turns out that the adsorption data for butyl benzoate were also ''intermediate'' between those observed for the other three compounds and were more difficult to model. As a consequence, experimental data were acquired with four different mobile phase compositions, 80:20; 70:30; 65:35 and 60:40 (v/v) of methanol–water. For solubility reasons, the range of concentrations in which the isotherm could be measured decreases with decreasing methanol concentration and was 0–17, 0–10, 0–8 and 0–6 g/dm^3, respectively. Because of the isotherm behavior is nearly linear, it is convenient to report the equilibrium data also as plots of q^*/C versus C since this illustrates more clearly the deviation from linear behavior.

4.5.1. Data with 80:20 (v/v) methanol–water

The plots of the equilibrium isotherm data obtained are nearly linear over the whole range of concentration. Fig. 7 shows a slight but definite convex upward shape. The isotherm chord (q^*/C) decreases rapidly with increasing concentration at low concentrations ($C<2$ g/dm^3), followed by a slower and linear decrease in the higher concentration range. The extrapolation of the first part of

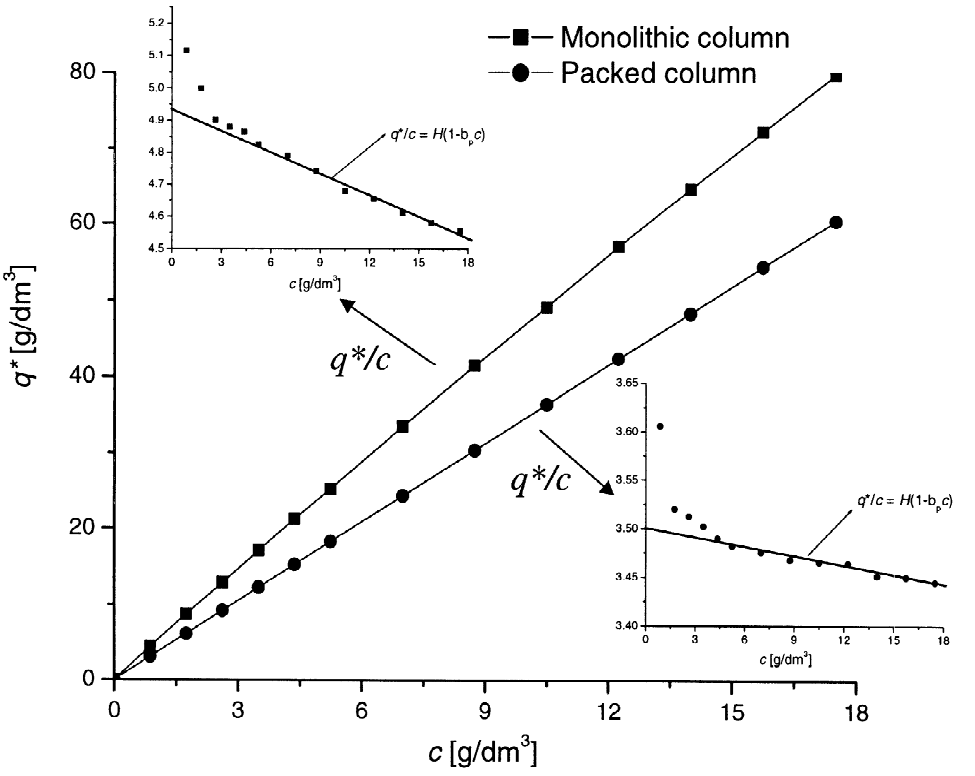

Fig. 7. Isotherm of butylbenzoate on the monolithic and the packed columns with methanol–water (80:20, v/v) as the mobile phase. Insert: plot of q^*/C as a function of C for both columns. $T = 295$ K.

the curve gives values of the Henry constant of 5.25 and 3.75 for the monolithic and the packed columns, respectively. The ratio between these two values is again approximately 1.4 in favor of the monolithic column. A parabolic isotherm would fit very well these data because the deviation from linear behavior is so small and any isotherm can be accounted for by the first two terms of its Taylor expansion at low concentrations. The second coefficient of this parabolic isotherm has no physical meaning and cannot be interpreted.

4.5.2. Data with 70:30, 65:35 and 60:40 (v/v) methanol–water

The data obtained are illustrated in Figs. 8, 9 and 10. These figures show both the isotherms as plots of q^*/C versus C and a series of breakthrough curves. The general aspects of these isotherms are different from the one obtained with the 80:20 composition, these three isotherms exhibiting a clear inflection point characterized by a minimum of the q^*/C versus C plot. The isotherm is convex downward at low concentrations and becomes convex upward at high concentrations. The breakthrough curves have a front shock layer at low concentrations, a diffuse boundary layer at high concentrations. However, beyond their inflection point, they raise much more slowly toward the limit plateau concentration than was observed for the three other compounds. The concentration at which the slope of the isotherm chord (q^*/C) is minimum decreases progressively with decreasing methanol concentration. This minimum takes place at slightly higher concentrations for the monolithic column with values of ca. 8, 5 and 2 g/dm^3 for compositions of 70:30; 65:35 and 60:40 (v/v) of methanol–water while these respective values are 6.5, 3.5 and 2 g/dm^3 for the packed column. This illustrates the limited influence of the

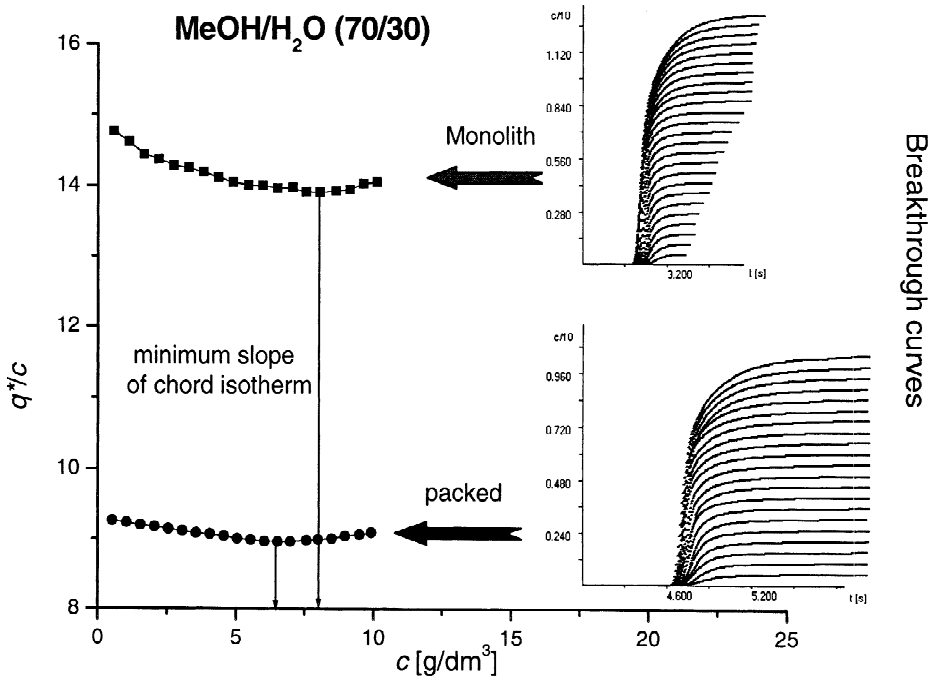

Fig. 8. Breakthrough curves of butylbenzoate and corresponding plot of q^*/C versus C with methanol–water (70:30, v/v) as the mobile phase. $T = 295$ K.

mobile phase composition on the isotherm: it controls the concentration of the inflection point of the isotherm, not its shape. The thermodynamics remains the same on both columns independently of the mobile phase composition.

Only specific isotherm models can account for this type of behavior. These are models that include solute–solute interactions in the adsorbed phase. The experimental data were fitted to several models. First, we used the following models, previously described by Quinones and Guiochon [53].

(1) *The Fowler model*, derived from statistical thermodynamics [54]. This is the simplest model assuming localized monolayer adsorption with lateral attractive interactions between solutes occupying two nearest-neighbor sites.

(2) *The N-polynomial model*, also derived from statistical thermodynamics [25]. Within this model, the adsorbate molecules are localized at different surface-independent sites (or cages), each site containing a maximum of N molecules.

(3) *The Kiselev model* [55]. This model assumes a set of quasi-chemical reversible reactions for the formation of *N*-dimensional associates or monolayer cluster. The Kiselev implicit model is obtained by assuming any possible dimension for the cluster.

The fitting of the experimental data for butylbenzoate to all three models was not successful. The regression analysis never converged toward a constant set of parameters with a good value of the Fisher parameter and a reasonably narrow confidence interval. Therefore, these isotherms models were rejected. The data were then fitted to the four isotherm models described earlier (see Section 2). In all cases convergence to a single solution for a set of the model parameters was achieved, with a very good agreement (Fisher coefficient of the order of 1×10^5). Tables 3 and 4 summarize the computational results of the regression analysis for each mobile phase composition and each isotherm model, the Fowler-Guggenheim/Jovanovic-Freundlich (FG/JF), the Langmuir/anti-Langmuir (LAL), the extended liquid–solid virial, and the B.E.T. isotherm models.

Although they gave high Fisher test values, the

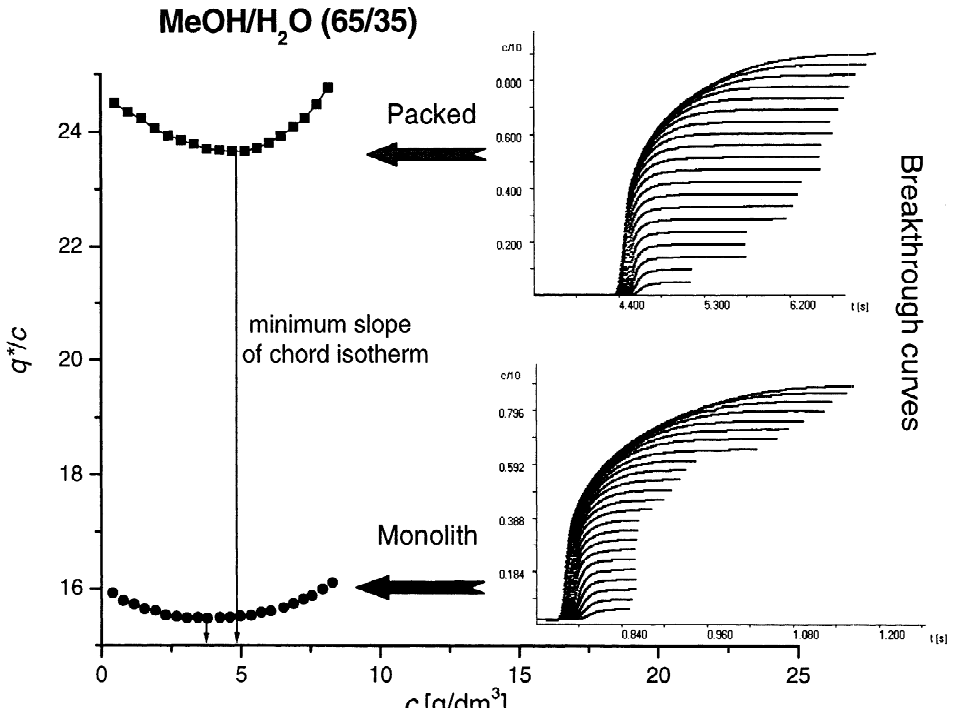

Fig. 9. Breakthrough curves of butylbenzoate and corresponding plot of q^*/C versus C with methanol–water (65:35, v/v) as the mobile phase. $T=295$ K.

confidence interval of the parameters of the FG/JF and AL/L models were not satisfactory. Furthermore, the evolution of these parameters with the mobile phase composition did not make any physical sense. Conversely, the extended liquid–solid virial and the B.E.T. models gave satisfactory results regarding the confidence interval of each parameter and the evolution of these parameters with changes in the mobile phase composition.

Admittedly, the B.E.T. isotherm model, a model that assumes an infinite number of adsorbed layers, might not be the best model to account for our experimental results. A still better agreement could possibly be obtained with a model assuming a finite number of layers. Fig. 11 shows a plot of the value of the Fisher test versus the number of adsorbed layers in intermediate models. Note that all these models have the same number of parameters, the number of layers, n, and the three parameters (q_S, b_S and b_L) of the BET model (Eq. (15)). Clearly, the Fisher parameter increases with n and tends toward a limit corresponding to the B.E.T. model. Similarly, the plots in Fig. 12 show that the parameters of n-multilayer isotherm models converge toward those of the B.E.T. model and the plots in Fig. 13 show that the relative confidence level of each coefficient decreases uniformly toward the value corresponding to the B.E.T. model.

Finally, it is noteworthy that the saturation capacity q_S found for butylbenzoate with the B.E.T. model is in good agreement with the capacities found for the hydroxyl compounds. These values are 210 and 145 g/dm^3 for the monolithic and the packed columns, respectively (versus 220 g/dm^3 for the alcohol and 270 g/dm^3 for the phenol on the monolithic column, 140 and 180 g/dm^3, respectively, on the packed column). More importantly still, the same values were determined for the two equilibrium constants of the BET model (b_S and b_L) on the two columns (Tables 3 and 4). These values depend on the mobile phase composition, not on the design of the stationary phase. Furthermore, the variation

Table 4
Packed silica particles column[a]

BET	Fisher	q_s	IC_{95} (%)	b_S	IC_{95} (%)	b_L	IC_{95} (%)		
60:40	9.95E+04	127.1	2.9	0.211	3.8	0.0850	1.6		
65:35	2.20E+05	164.1	3.2	0.098	3.7	0.0396	2.2		
70:30	1.59E+05	129.7	5.6	0.073	6.1	0.0280	4.5		
FG/LF	Fisher	q_s	IC_{95} (%)	b_S	IC_{95} (%)	α	IC_{95} (%)	v	IC_{95} (%)
60:40	3.1E+08	1833.0	77.0	0.023	78	3.44	73.8	2.19	11.7
65:35	3.6E+05	547.0	24.0	0.046	25	1.31	16.2	2.13	6.8
70:30	1.2E+05	729.2	36.3	0.021	37	2.22	50.2	3.33	36.6
LAL	Fisher	q_{s1}	IC_{95} (%)	b_S	IC_{95} (%)	H_2	IC_{95} (%)	b_{aL}	IC_{95} (%)
60:40	1.2E+05	207.2	11.3	0.086	43	8.64	27.1	0.093	9.8
65:35	4.0E+05	445.3	9.2	0.028	32	3.28	37.1	0.054	13.8
70:30	1.6E+05	355.7	17.4	0.022	62	1.45	100.1	0.045	37.0
Virial	Fisher	H	IC_{95} (%)	A_1	IC_{95} (%)	A_2	IC_{95} (%)		
60:40	5.8E+04	26.04	0.9	5.94E-04	30.1	−8.74E-06	9.2		
65:35	9.2E+05	15.92	0.2	9.44E-04	5.6	−7.67E-06	3.8		
70:30	1.7E+05	9.43	0.6	1.76E-03	11.2	−1.47E-05	10.8		

[a] Adsorption of butylbenzoate compound. Fisher test values, isotherm parameters and their associated 95% confidence interval obtained by regression analysis on four models (B.E.T., FG/JF, LAL and virial) for three different mobile phase compositions of methanol–water mixtures (v/v).

trends of b_S and b_L are physically justified: the higher the volume fraction of methanol in the mobile phase, the higher the solubility of butylbenzoate, and the lower are its two adsorption–desorption equilibrium constant, the one with the surface and the one with the underlying adsorbed layer. For methanol concentrations of 70, 65, and 60%, the b_S values are 0.21, 0.11 and 0.07, respectively, and the values of b_L 0.085, 0.042 and 0.027, respectively.

4.5.3. Validation of isotherm models for butylbenzoate

One of the most sensitive test of the quality of an isotherm model is the accuracy with which they can

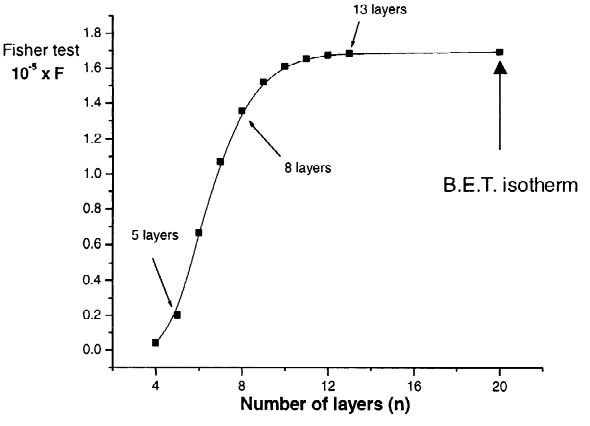

Fig. 11. Plots of the Fisher test value (F) obtained when fitting the experimental data to a series of successive n-multilayer models versus n. Butylbenzoate, packed C_{18} column, methanol–water (65:35, v/v). $T = 295$ K.

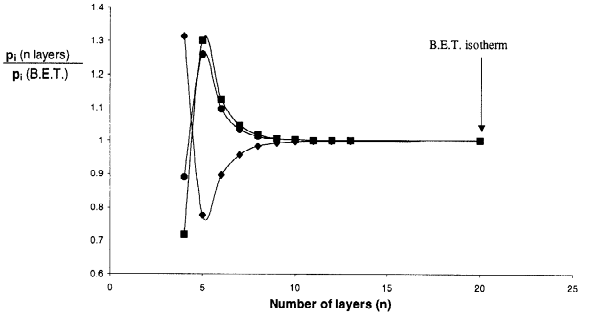

Fig. 12. Plot of the isotherm parameters p_i of the n-multilayer model normalized to those of the B.E.T. model versus the number of layers, n. (♦) q_S, (●) b_L, (■) b_S. Butylbenzoate, packed C_{18} column, methanol–water (65:35, v/v). $T = 295$ K.

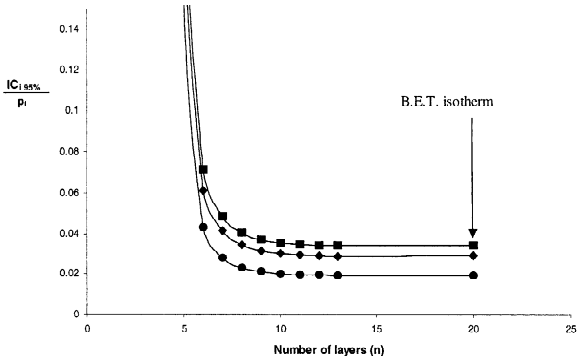

Fig. 13. Plot of the relative confidence interval (Student 95%) for the three parameters p_i of the n-multilayer model versus the number of layers, n. (♦) q_S, (●) b_L, (■) b_S. Butylbenzoate, packed C_{18} column, methanol–water (65:35, v/v). $T = 295$ K.

model the chromatography process. For this purpose, the isotherm model should be coupled with a proper dynamic model to calculate band profiles. The validity of the isotherm model is confirmed only if it is able accurately to predict the profiles of elution bands and breakthrough curves in the whole range of concentrations that can be reached. Band profiles of butylbenzoate were calculated with each one of the isotherm models selected and the results were compared with the experimental profiles obtained under different process conditions. The calculations were performed using both the ED and the POR models.

The following combination of operating parameters were considered:

(1) Columns: monolithic and packed columns;

(2) Mobile phase (MeOH–H_2O) composition: 60:40; 65:45; 70:30 (v/v);

(3) The loading factor L_f was varied by changing the feed concentration and/or the volume injected.

4.5.3.1. Selection of the isotherm model (LaL; virial or B.E.T.) for both batch systems

The calculations were performed using the following three isotherm models selected for reasons explained earlier: the modified biLangmir isotherm (LaL isotherm), the virial isotherm and the B.E.T. isotherm models. For all these models, similar values of the Fisher test parameter were obtained (see Tables 3 and 4). Calculations were performed first with all the isotherm equations selected, using the ED model. The results obtained are compared to the experimental data in Fig. 14a,b. Obviously, the agreement between experimental and calculated chromatograms is excellent or very good when either the B.E.T. or the LaL isotherm is used. It is rather poor for the virial isotherm, for both columns. Note that:

(1) The profiles calculated with the virial isotherm differ markedly from the experimental ones, both in retention time and in shape. The evolution of these

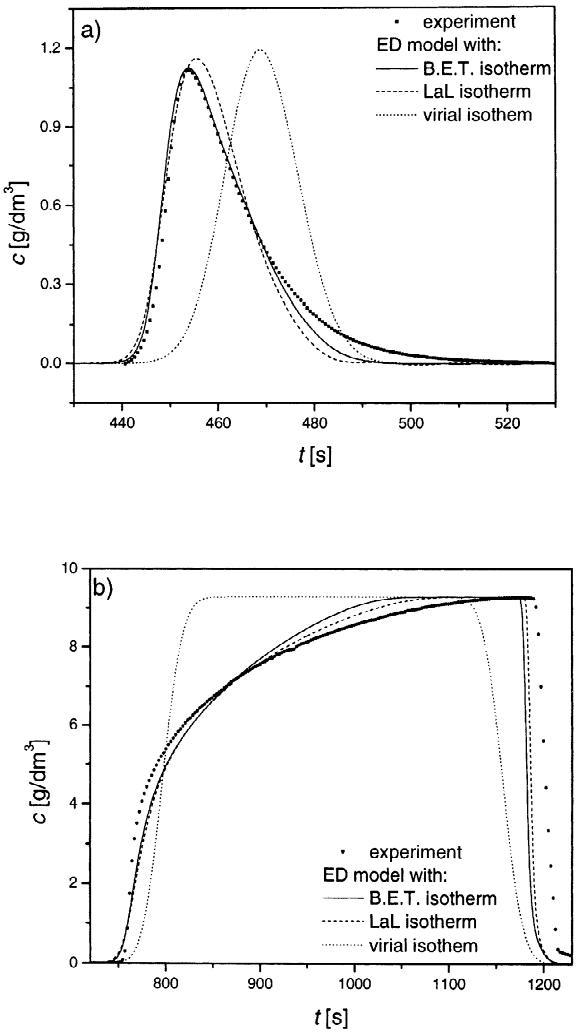

Fig. 14. Comparison between calculated and experimental band profiles. ED model and different isotherm models. Mobile phase composition: 65:35 (v/v). Packed column. (a) $C_0 = 4.70$ g/cm^3; $t_p = 4.8$ s; $L_f = 0.12\%$; $N = 3950$; (b) $C_0 = 9.56$ g/cm^3; $t_p = 360$ s; $L_f = 34.3\%$; $N = 1600$.

calculated profiles with increasing loading factor deviates markedly from experimental observations. This was surprising because the fitting of the isotherm data to this model gave coefficients determined with a very good precision (see Tables 3 and 4). This isotherm model was eliminated from the further study.

(2) For the LaL isotherm a good or very good agreement between calculated and experimental band profiles was achieved. However, because the coefficients of this model have no clear physical meaning, we did not pursue further any investigation of this isotherm model.

4.5.3.2. Validation of the B.E.T. isotherm model using the ED Model

Series of band profiles were acquired in which the experimental conditions were varied systematically. These profiles are compared to those calculated using the ED model and the B.E.T. isotherm. Figs. 15–19 show the elution profiles obtained for several injections at different values of the loading factor L_f and under different conditions. The agreement between calculated and experimental profiles is excellent under all conditions, for both columns, particularly for the diffuse rear boundaries. In the case of the front shock layers, the agreement was found to be slightly better for the packed than for the monolithic column. As examples of these results, Fig. 15a,b compares the experimental chromatograms and those calculated with the ED and the POR models. Other figures (Figs. 16–19) illustrate several thermodynamics and kinetics issues in the chromatographic system investigated.

Figs. 14 and 15 show that, in most cases, the band profiles calculated with the B.E.T. isotherm model account very well for the experimental profiles. However, under certain conditions, differences are observed between the experimental and the calculated chromatograms. The following conclusions are derived from a detailed study of these differences.

(1) The agreement between experimental and the calculated chromatograms is excellent for moderate values of L_f, particularly at 65:35 (v/v) (Fig. 14a,b).

(2) This agreement depends on the mobile phase concentration. The best agreement is observed for a composition of 65:35 (v/v) (Fig. 14a,b). It is slightly less good for 60:40 and 70:30 (v/v) (Figs. 15a,b and 18a,b).

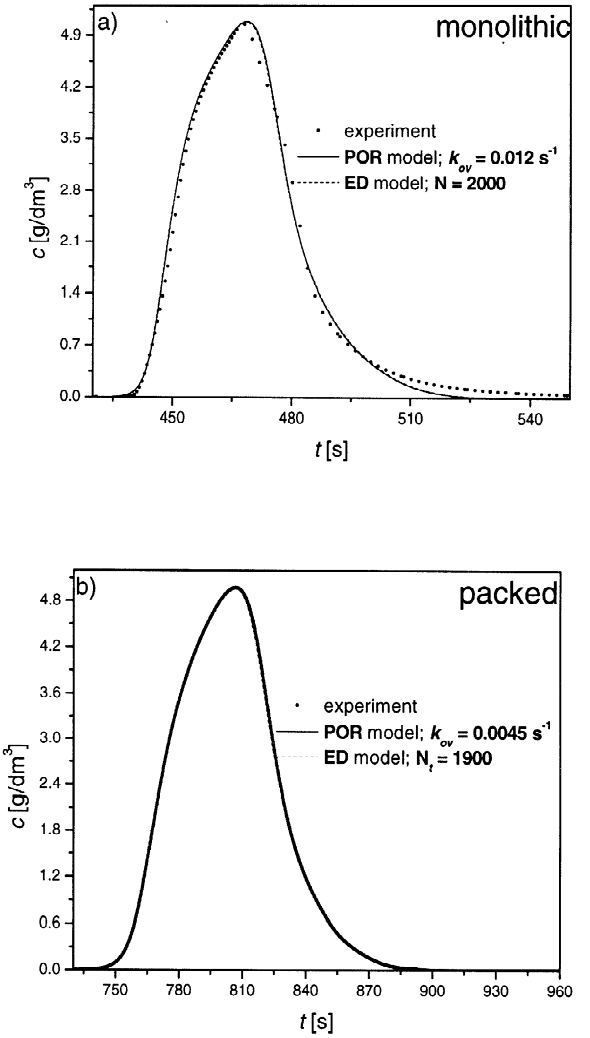

Fig. 15. Comparison between calculated and experimental band profiles. ED and POR models, B.E.T. isotherm equation. Mobile phase composition: 65:35 (v/v). (a) Monolithic column: C_0 = 8.56 g/cm^3; t_p = 19.2 s; L_f = 0.94%. (b) Packed column: C_0 = 6.89 g/cm^3; t_p = 42 s; L_f = 2.88%.

(3) This agreement is only reasonably good at very low and low values of the loading factor L_f (Fig. 16).

(4) This agreement is fairly good at high and very high L_f (Fig. 17).

(5) For strongly overloaded conditions, when the injection plateau is not entirely eroded, and for

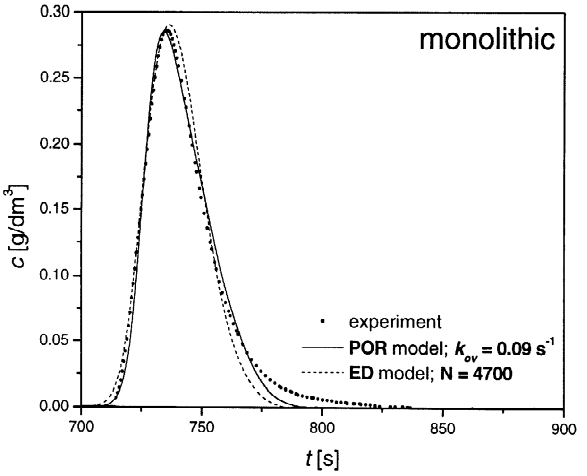

Fig. 16. Comparison between calculated and experimental band profiles. ED and POR models, B.E.T. isotherm equation, monolithic column. Mobile phase composition: 60:40 (v/v). $C_0 = 1.80$ g/cm^3; $t_p = 4.8$ s; $L_f = 0.05\%$.

breakthrough curves, there are systematic differences between the calculated profiles that exhibit sharp fronts with thin shock layers while the recorded profiles show a smoother transition from the less steep front to the plateau (Fig. 19a,b).

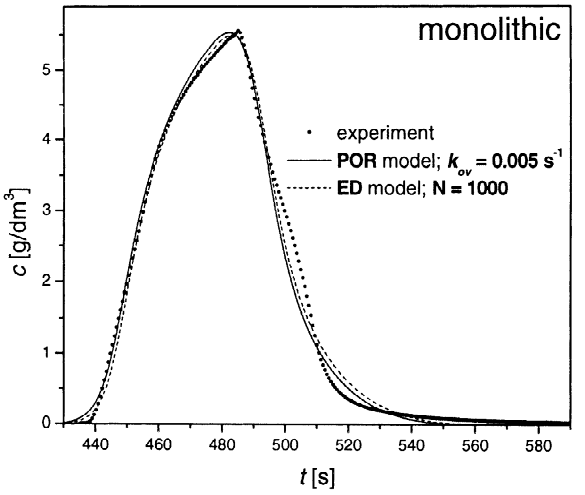

Fig. 17. Comparison between calculated and experimental band profiles. ED and POR models, B.E.T. isotherm equation, monolithic column. Mobile phase composition: 65:35 (v/v). $C_0 = 10.70$ g/cm^3; $t_p = 24$ s; $L_f = 1.46\%$. Note the artifactual hump on the rear boundary of the profile (see text).

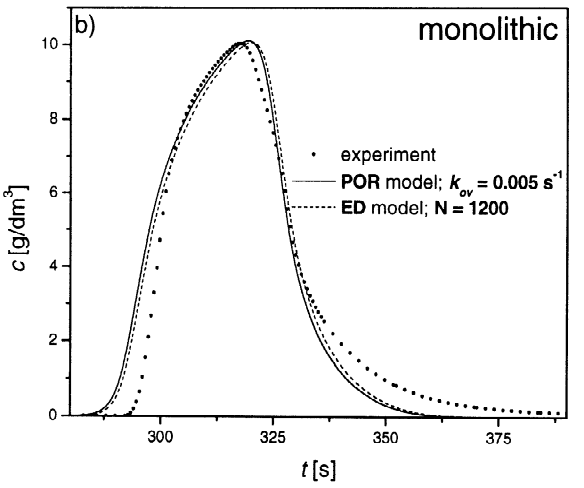

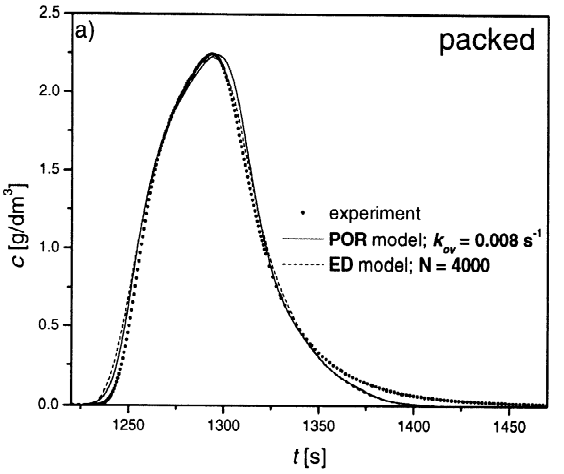

Fig. 18. Comparison between calculated and experimental band profiles. ED and POR models, B.E.T. isotherm equation. Illustration of the influence of the modifier concentration (see results for 65:35 (v/v), mobile phase composition in Fig. 16a,b). (a) Mobile phase composition: 60:40 (v/v), $C_0 = 3.59$ g/cm^3; $t_p = 42$ s; $L_f = 1.94\%$; (b) Mobile phase composition: 70:30 (v/v), $C_0 = 13.2$ g/cm^3; $t_p = 24$ s; $L_f = 1.85\%$;.

The comparison between experimental and calculated chromatograms reveals also some systematic errors:

(1) At low values of the loading factor, the experimental profiles elute faster than predicted.

(2) At high values of the loading factor, the

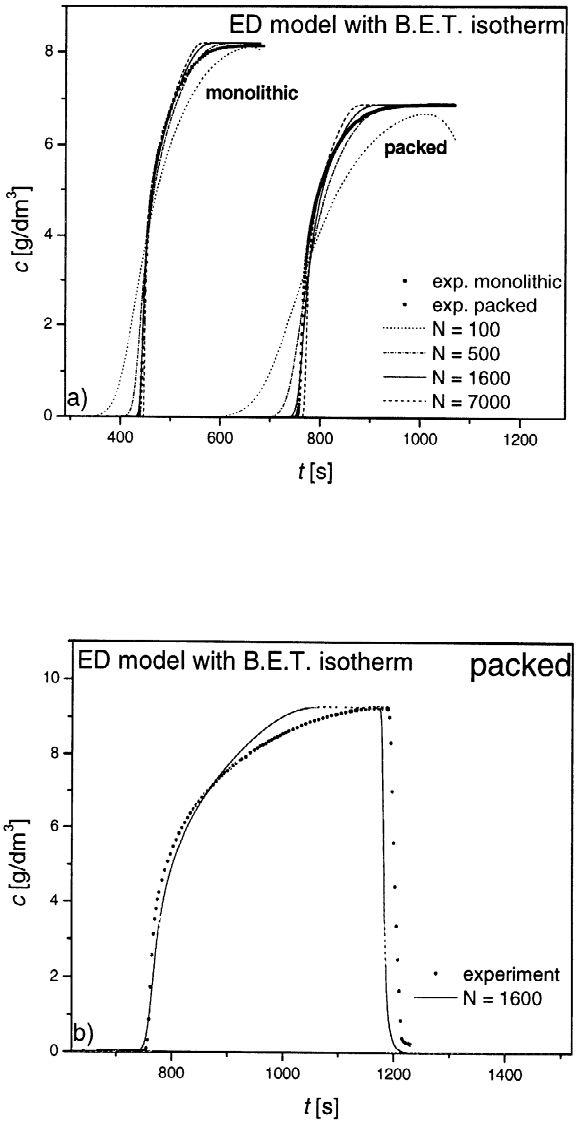

Fig. 19. Comparison between calculated and experimental band profiles under strongly overloaded conditions. ED and POR models, B.E.T. isotherm equation. Breakthrough curves for 65:35 (v/v). (a) Monolithic column: $C_0 = 8.56$ g/cm^3; $t_p = 270$ s; $L_f = 13.2\%$. Packed column: $C_0 = 6.89$ g/cm^3; $t_p = 360$ s; $L_f = 24.7\%$. (b) Packed column: $C_0 = 9.56$ g/cm^3; $t_p = 360$ s; $L_f = 34.3\%$.

experimental profiles elute more slowly than predicted.

These errors arise from discrepancies between the best B.E.T. isotherm model and the experimental data in the low and the high ranges of concentrations. The retention times of the bands and their profiles are very sensitive to small changes in the values of the isotherm coefficients. For example, a change of the value of b_S (Tables 3 and 4) by $\pm 3\%$ alters the retention times by ± 3–10%.

Besides these differences arising from the thermodynamics inaccuracy of our model, two other phenomena caused difficulties in accounting correctly for experimental profiles:

(1) The experimental band profiles are followed by a long diffuse tail which is not predicted by the calculated profiles (see Figs. 17–19b). This peak tailing results from back-mixing that takes place in the solvent delivery system, probably the pump. If an injector is used instead, to record the elution bands of small-volume samples, the profiles exhibit no peak tailing.

(2) Elution bands obtained upon injection of highly concentrated samples on the monolithic column exhibit the characteristic hump seen on the peak tail in Fig. 18. This hump disappears when the column has been washed under a stream of methanol for an extended period of time. Great care should be taken to filter the mobile phase and samples when using monolithic columns. This observation is at variance with those made by many analysts. The apparent contradiction may be explained by the different nature of the samples handled.

Finally, note that, in all these comparisons, the good to excellent agreement observed between calculated and experimental profiles was achieved only because the number of theoretical plates used in the ED model was optimized in each particular case. This optimum number decreases with increasing concentration of methanol in the mobile phase and with increasing loading factor, as illustrated in Table 5. Such a decrease indicates that the mass transfer kinetics, not axial diffusion, controls band broadening and that it is not properly accounted for in the ED model [56]. Despite the relatively high efficiency of the two columns, the ED model appears not to be accurate enough to account for the kinetic effects.

4.5.3.3. Validation of B.E.T. isotherm model using the POR Model

Because of the high column efficiency, the band profiles calculated using the most accurate general rate model of chromatography (GR) and the simplified POR model are expected to be the same. The

Table 5
POR model parameters used for the estimation of k_{ov}

Parameter	Mobile phase composition (v/v)			Origin
	60:40	65:35	70:30	
Molecular diffusion coefficient, D_m (cm^2/s)	4.41e-6	4.46e-6	4.66e-6	[39]
Dispersion coefficient, D_L (cm^2/s)	1.126e-4	1.125e-4	1.121e-4	[37]
	Monolithic		Packed	
Total porosity, ε_T	0.844		0.570	Uracil
External porosity, ε_e	0.690		0.370	[50]
Internal porosity, ε_p	0.497		0.328	Calc.

overall mass transport rate coefficient is given by Eq. (22). While the molecular diffusivity, D_m, is easily calculated (see Eq. (24)) and is known with a reasonable precision, accurate estimates of the external mass transfer rate coefficient, k_{ext}, and of the axial dispersion coefficient, D_L, that are both necessary to calculate band profiles with the POR models, are more difficult to obtain.

According to Wilson and Geankoplis [57], k_{ext} can be estimated from the following correlation:

$$\mathrm{Sh} = \frac{k_{ext} d_p}{D_m} = \frac{1.09}{\varepsilon_e} (\mathrm{Sc\ Re})^{0.333} \quad (27)$$

The Reynolds (Re) and Schmidt (Sc) numbers are defined in Eq. (23).

The column Peclet number [58] exceeds 2100 for the packed column and 1400 for the monolithic column [23] and the ratio St/Bi is equal to about 115 for the packed column and 210 for the monolithic column [23]. Thus, the conditions of equivalence of the GR and the POR model derived by Kaczmarski and Antos [58] are satisfied and the use of the POR model is justified.

The remaining parameters of the POR model were calculated and presented in Table 5. The values of the overall mass transfer rate coefficient, k_{ov}, were determined by parameter identification, as was the number of theoretical plates in the ED model (see previous section). The results of the exercise are reported in Table 6. Comparison of experimental band profiles and of those calculated with the POR

Table 6
Best efficiency (N) and overall mass transfer coefficient (k_{ov}) obtained for various overloaded profiles and mobile phase composition

Mobile phase MeOH–H_2O (v/v)	Monolith					Packed				
	Injection			ED N	POR k_{ov} (s^{-1}) $\times 10^3$	Injection			ED N	POR k_{ov} (s^{-1}) $\times 10^3$
	c_0 (g/dm^3)	t_p (s)	L_f[a] (%)			c_0 (g/dm^3)	t_p (s)	L_f[a] (%)		
60:40	1.80	4.8	0.05	4700	90	1.79	12	0.28	5000	14
	4.13	19.2	0.46	2700	24	3.59	42	1.94	4000	8
65:35	4.70	4.80	0.12	3950	–	3.82	42	1.6	2400	5.5
	4.70	16.2	0.43	2850	20	6.89	42	2.88	1900	4.5
	8.56	19.2	0.94	2000	12	6.89	360	24.7	1600	–
	8.56	270	13.2	1600	–	9.56	42	4.00	1600	3.5
	10.70	24	1.46	1000	5	9.56	360	4.00	1600	–
70:30	5.45	4.8	0.15	2200	10	5.24	12	0.79	1700	4
	13.20	24	1.85	1200	5	12.06	66	10.0	1000	1.2

[a] $L_f = c_0 t_p\ Fl/(q_s \varepsilon_t V_{col})$.

model reveals similar accuracy in the prediction of the experimental band profiles as was achieved previously with the ED model. In most cases, the profiles calculated by the ED and by the POR models are in close agreement.

The values of the overall mass transport rate coefficient decrease with increasing sample size. These values depend also on the methanol concentration of the mobile phase. These variations of k_{ov} can be explained only by a variation of the internal mass transfer coefficient which, in turn, depends on the surface diffusion coefficient. This result suggests that surface diffusion plays an important role in the mass transfer mechanism in both columns. Surface diffusion, however, is accounted for neither in the ED nor in the POR models. The analysis of the detailed mass transfer mechanism in the elution of the compounds studied here is outside the scope of this work and will be reported on later.

4.6. Comparison of the preparative performance of the two columns

The results obtained with the four compounds studied show that the saturation capacity of the monolithic column is larger than that of the packed column by a factor close to 1.4 while the binding constants are nearly the same on both columns. This result is valid independently of the nature of the compound and of the isotherm model to which its adsorption equilibrium data fit best. It suggests that the chemistry of both surfaces are very similar and that the effective surface area contained in the monolithic column is approximately 40% larger than that contained in the conventional packed column.

Some of the consequences of this conclusion are illustrated in Fig. 20 which shows chromatograms of large samples of mixtures of butylbenzoate and 4-*tert*.-butylphenol (Fig. 20a,b) and of butylbenzoate and butylbenzene (Fig. 20c,d). The amounts injected were proportional to the amounts of C_{18} chains contained in each column, i.e., to their weights of packing material. So, the injected sample size was three times larger on the packed than on the monolithic column. For each chromatogram, the following parameter, P_C, was calculated:

$$P_C = \frac{t_2 - t_1}{2\omega_{1,2}} \quad (28)$$

where $\omega_{1,2}$ is the half-height time width of the first eluted peak and t_1 and t_2 are the retention times of the fronts of the first and second compounds, respectively. P_C is a modified resolution factor. Since the selectivity and efficiency of the two columns are the same, differences between the values of P_C depend only on their effective saturation capacity. Yet, the data in Table 7 show that P_C is systematically at least 1.3 times higher on the monolithic than on the packed column, which illustrates the higher saturation capacity of the former column and confirms the results of FA measurements. From a practical viewpoint, one can inject 30–40% more sample per unit mass of stationary phase on the monolithic column and obtain the same degree of separation as on a classical packed column. Because of the difference in density between the two columns, however, the loadability of a standard packed column is higher than that of a monolithic column of the same size.

5. Conclusion

Our results demonstrate that, for four compounds having different polarities and retention mechanisms, the chemistry of the surface of the first commercially available monolithic C_{18} bonded silica column is closely similar to that of a typical conventional column packed with small particles. This result was not unexpected and seems quite reasonable. Accordingly, it can be assumed that it is fairly general. Yet, the close agreement between the values of the binding constants measured on the two columns is impressive and noteworthy.

More surprising is the fact that the specific saturation capacities for these four compounds, i.e., the saturation capacities measured for the columns and reported to the unit mass of packing material (or, for that matter, to the amount of C_{18} chains in the column), are markedly larger on the monolithic than on the packed column, even though the two silica materials have close specific surface areas and carbon content. This observation contrasts with the nearly identical surface chemistry of the two surfaces. This comparison suggests that the effective or accessible surface area of the monolithic column is larger than that of the packed column. Hence, it seems probable that the marked differences between

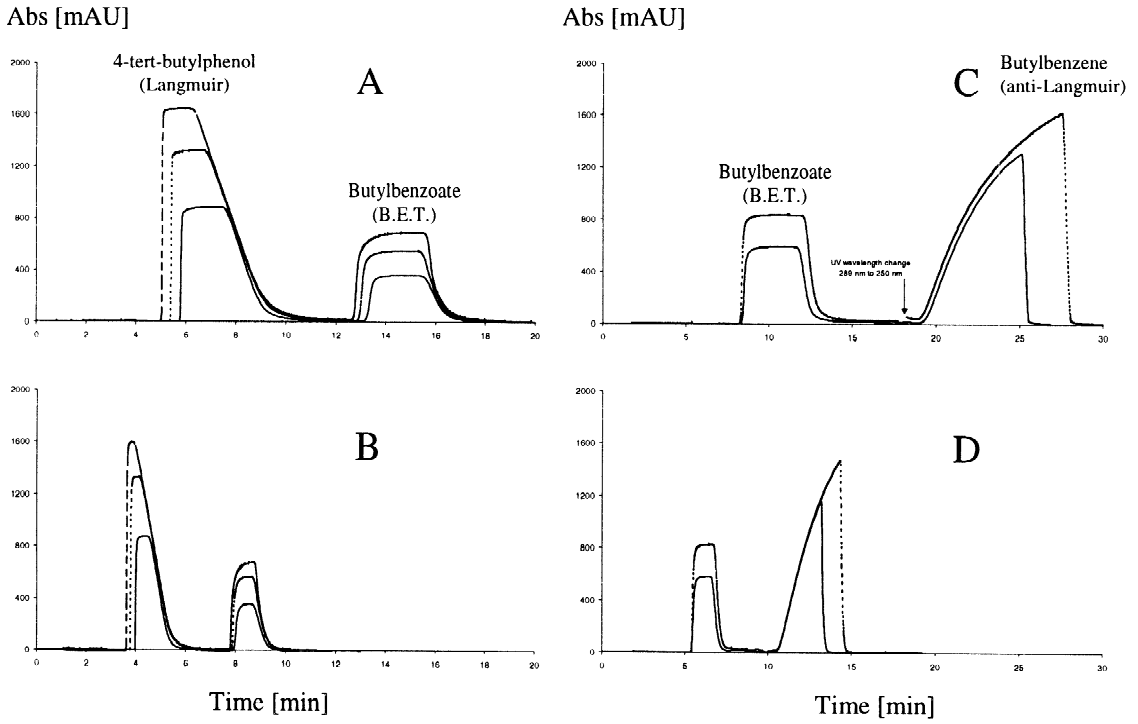

Fig. 20. Chromatograms obtained upon the injection of two binary mixtures in amounts proportional to the amount of C_{18} chains in the monolithic (B,D) and the packed (A,C) columns. Separations of 4-*tert*.-butyphenol and butylbenzoate (A,B, $\lambda = 290$ nm for both solute) and of butylbenzoate and butylbenzene (C,D, $\lambda = 289$ nm for butylbenzoate then $\lambda = 250$ nm for butylbenzene). Mobile phase composition of 65:35 (A,B) and 70:30 (C,D) (v/v) methanol–water. Flow rate, 1 ml/min, $T = 295$ K. (a) Injection of 2.40 cm^3 of solutions at concentrations 2, 4 and 6 g/dm^3 for the solutes, respectively. (b) Injection of 0.80 cm^3 of the same solutions as in (a). (c) Injection of 3.36 cm^3 of solutions at concentrations 2.5 and 5 g/dm^3 for the solutes, respectively. (c) Injection of 1.12 cm^3 of the same solutions as in (c).

the structure of the pore network, the accessibility of the surface to the adsorbate molecules, and the pore connectivity might explain these differences.

On the theoretical front, this result could be related to those obtained by Meyers and co-workers who simulated the pore networks of monolithic and packed columns [59]. They showed that the dynamic adsorptive capacity behavior of the monolithic column was always greater than that of different packed beds [60] and that the differences between them increased with increasing particle size and increasing mobile phase velocity. The monolithic porous silica is possibly characterized by a high connectivity between its large macropores and the mesopores, allowing a more efficient transport of the solutes and access to a larger fraction of the total surface area.

Table 7
Values of the factor P_C obtained on the monolith and packed columns for the separations of the studied compounds presented in Fig. 20

Separation	C_0 (g/dm^3)	MP (v/v)	P_C Packed	P_C Monolithic	$P_{C\,Monolith}/P_{C\,Packed}$
4-*tert*.-Butylphenol–butylbenzoate	2.0	65:35	1.46	2.06	1.41
	4.0		1.41	1.95	1.38
	6.0		1.39	1.90	1.37
Butylbenzoate–butylbenzene	2.5	70:30	1.46	1.90	1.30
	5.0		1.29	1.73	1.34

Conversely, the high tortuosity of the stream pathways as well as the existence of frequent constrictions in the packed silica bed may reduce effective accessibility of the adsorption surface to the solutes.

On the practical front, the apparent surface area of a monolithic column is 40% higher than that of a packed column while it can easily be operated at a 40% higher flow velocity or at a faster one while affording the same efficiency as the conventional column. These characteristics more than compensate for the lower total surface area contained in a column of given volume. Therefore, this new column type offers some potential advantages in terms of production rate.

Acknowledgements

This work was supported in part by grant CHE-00-70548 of the National Science Foundation and by the cooperative agreement between the University of Tennessee and the Oak Ridge National Laboratory. We thank Karin Sinz, Karin Cabrera, Dieter Lubda (Merck KGaA, Darmstadt, Germany) and Fred Rabel (EM Science, Gibbstown, NJ, USA) for the generous gift of the columns used in this work and for fruitful discussions.

References

[1] J.C. Giddings, in: Unified Separation Science, Wiley, New York, 1991.
[2] P.A. Bristow, J.H. Knox, Chromatographia 10 (1977) 279.
[3] H. Poppe, J. Chromatogr. A 778 (1997) 3.
[4] H. Minakuchi, K. Nakanishi, N. Soga, N. Ishizuka, N. Tanaka, Anal. Chem. 68 (1996) 3498.
[5] H. Minakuchi, K. Nakanishi, N. Soga, N. Ishizuka, N. Tanaka, J. Chromatogr. A 762 (1997) 135.
[6] H. Minakuchi, K. Nakanishi, N. Soga, N. Ishizuka, N. Tanaka, J. Chromatogr. A 797 (1998) 121.
[7] N. Ishizuka, H. Minakuchi, K. Nakanishi, N. Soga, N. Tanaka, J. Chromatogr. A 797 (1998) 133.
[8] H. Minakuchi, K. Nakanishi, N. Soga, N. Ishizuka, N. Tanaka, J. Chromatogr. A 828 (1998) 83.
[9] N. Ishizuka, H. Minakuchi, K. Nakanishi, N. Soga, N. Tanaka, J. Chromatogr. A 797 (1998) 133.
[10] N. Tanaka, H. Nagayama, H. Kobayashi, T. Ikegumi, K. Hosoya, N. Ishizuka, H. Minakuchi, K. Nakanishi, K. Cabrera, D. Lubda, J. High Resolut. Chromatogr. 23 (2000) 111.
[11] K. Cabrera, G. Wieland, D. Lubda, K. Nakanishi, N. Soga, H. Minakuchi, K.K. Unger, Trends Anal. Chem. 17 (1998) 50.
[12] K. Cabrera, D. Lubda, H.-M. Eggenweiler, H. Minakuchi, K. Nakanishi, J. High Resolut. Chromatogr. 23 (2000) 93.
[13] N. Ishizuka, H. Minakuchi, K. Nakanishi, K. Hirao, N. Tanaka, Colloids Surfaces A: Physicochem. Eng. Aspects 187–188 (2001) 273.
[14] B. Bidlingmaier, K.K. Unger, N. von Doehren, J. Chromatogr. A 832 (1999) 11.
[15] M. Kele, G. Guiochon, J. Chromatogr. A 960 (2002) 19.
[16] D. Josic, A. Buchacher, A. Jungbauer, J. Chromatogr. B 752 (2001) 191.
[17] P. Zöllner, A. Leitner, D. Lubda, K. Cabrera, W. Lindner, Chromatographia 52 (2000) 818.
[18] G. Dear, R. Plumb, D. Mallett, Rapid. Commun. Mass Spectrom. 15 (2001) 152.
[19] K. Cabrera, D. Lubda, H.-M. Eggenweiler, H. Minakuchi, K. Nakanishi, J. Chromatogr. A 762 (1997) 135.
[20] M. Schulte, D. Lubda, A. Delp, J. Dingenen, J. High Resolut. Chromatogr. 23 (2000) 100.
[21] M. Schulte, J. Dingenen, J. Chromatogr. A 923 (2001) 17.
[22] L. Spoof, J. Meriluoto, J. Chromatogr. A 947 (2002) 237.
[23] A. Cavazzini, G. Bardin, K. Kaczmarski, P. Szabelski, M. Al-Bokari, G. Guiochon, J. Chromatogr. A 957 (2002) 111.
[24] G. Guiochon, S. Golshan-Shirazi, A.M. Katti, in: Fundamentals of Preparative and Nonlinear Chromatography, Academic Press, Boston, MA, 1994.
[25] D.M. Ruthven, in: Principles of Adsorption and Adsorption Processes, Wiley, New York, NY, 1984.
[26] S. Golshan-Shirazi, G. Guiochon, J. Chromatogr. 506 (1990) 495.
[27] R.M. Barrer, J.A. Davies, Proc. R. Soc. London A 320 (1970) 289.
[28] A.P. Vavlitis, D.M. Rurhven, K.F. Loughlin, J. Colloid Interface Sci. 84 (1981) 526.
[29] I. Quinones, G. Guiochon, J. Chromatogr. A 196 (1998) 15.
[30] S. Brunauer, P.H. Emmet, E. Teller, J. Am. Chem. Soc. 60 (1938) 309.
[31] D.M. Youg, A.D. Crowell, in: Physical Adsorption of Gases, Butterworths, London, 1962.
[32] F.E. Bartell, D.J. Donahue, J. Phys. Chem. 56 (1952) 665.
[33] L.E. Brecher, J.A. Kostecki, D.T. Camp, Physical Adsorption Processes Principles 63 (1967) 18.
[34] L.E. Brecher, D.C. Frantz, J.A. Kostecki, Physical Adsorption Processes Principles 63 (1967) 25.
[35] R.M. McCormick, B.L. Karger, Anal. Chem. 52 (1980) 2249.
[36] M. Suzuki, in: Adsorption Engineering, Elsevier, Amsterdam, 1990.
[37] D. Gunn, Chem. Eng. Sci. 42 (1987) 363.
[38] C.R. Wilke, P. Chang, AICHE J. 1 (1955) 264.
[39] L.R. Perkins, C.J. Geankoplis, Chem. Eng. Sci. 24 (1969) 1035.
[40] H.S. Tsou, E.E. Graham, AICHE J. 31 (1985) 1959.
[41] E.E. Graham, C.F. Fook, AICHE J. 28 (1982) 245.
[42] G.L. Skidmore, B.J. Horstmann, A.H. Chase, J. Chromatogr. 498 (1991) 113.

[43] M.A. Fernandez, G. Carta, J. Chromatogr. A 746 (1996) 169.
[44] H. Yoshida, M. Yoshikawa, T. Kataoka, AICHE J. 40 (1994) 2134.
[45] P.W. Danckwerts, Chem. Eng. Sci. 2 (1953) 1.
[46] K. Kaczmarski, M. Mazzotti, G. Storti, M. Morbidelli, Comput. Chem. Eng. 21 (1997) 641.
[47] K. Kaczmarski, Comput. Chem. Eng. 20 (1996) 49.
[48] K. Kaczmarski, D. Antos, J. Chromatogr. A 862 (1999) 1.
[49] P.N. Brown, A.C. Hindmarsh, G.D. Byrne, Procedure available from: http://www.netlib.org.
[50] M. Al-Bokari, D. Cherrak, G. Guiochon, J. Chromatogr. A 975 (2002) 275.
[51] M. Kele, G. Guiochon, J. Chromatogr. A 830 (1999) 55.
[52] R.J. Smith, C.S. Nieass, M.S. Wainwright, J. Chromatogr. 9 (1986) 1387.
[53] I. Quiñones, G. Guiochon, Langmuir 12 (1996) 5433.
[54] R.H. Fowler, E.A. Guggenheim, in: Statistical Thermodynamic, Cambridge University Press, Cambridge, 1960.
[55] G.I. Berezin, A.V. Kiselev, J. Colloid Interface Sci. 38 (1972) 227.
[56] K. Kaczmarski, D. Antos, H. Sajonz, P. Sajonz, G. Guiochon, J. Chromatogr. A 925 (2001) 1.
[57] E.J. Wilson, C.J. Geankoplis, Ind. Eng. Chem. (Fund.) 5 (1966) 9.
[58] K. Kaczmarski, D. Antos, J. Chromatogr. A 756 (1996) 73.
[59] J.J. Meyers, A.I. Liapis, J. Chromatogr. A 852 (1999) 3.
[60] A.I. Liapis, J.J. Meyers, O.K. Crosser, J. Chromatogr. A 865 (1999) 13.